

Location Information Assisted Beamforming Design for Reconfigurable Intelligent Surface Aided Communication Systems

Zhe Xing, *Graduate Student Member, IEEE*, Rui Wang, *Senior Member, IEEE*, Xiaojun Yuan, *Senior Member, IEEE*, and Jun Wu, *Senior Member, IEEE*

Abstract—In reconfigurable intelligent surface (RIS) aided millimeter-wave (mmWave) communication systems, in order to overcome the limitation of the conventional channel state information (CSI) acquisition techniques, this paper proposes a location information assisted beamforming design without the requirement of the conventional channel training process. First, we establish the geometrical relation between the channel model and the user location, based on which we derive an approximate CSI error bound based on the user location error by means of Taylor approximation, triangle and power mean inequalities, and semidefinite relaxation (SDR). Second, for combating the uncertainty of the location error, we formulate a worst-case robust beamforming optimization problem. To solve the problem efficiently, we develop a novel iterative algorithm by utilizing various optimization tools such as Lagrange multiplier, matrix inversion lemma, SDR, as well as branch-and-bound (BnB). Particularly, the BnB algorithm is modified to acquire the phase shift solution under an arbitrary constraint of possible phase shift values. Finally, we analyse the algorithm complexity, and carry out simulations to validate the theoretical derivation of the CSI error bound and the robustness of the proposed algorithm. Compared with the existing non-robust approach and the robust beamforming techniques based on S-procedure and penalty convex-concave procedure (CCP), our method converges faster and achieves better performance in terms of the worst-case signal-to-noise ratio (SNR) at the receiver.

I. INTRODUCTION

For decades, the rapid development of telecommunication technologies has been concomitant with a surge of mobile data traffic along with a sharp increase in the number of mobile terminals, which sparks off a burning issue of spectrum scarcity. To deal with this issue, several key enabling techniques, such as millimeter-wave (mmWave), massive multiple-input-multiple-output (MIMO) and ultra-dense network (UDN), have been incorporated into the fifth-generation (5G) wireless communication network [1]. Although these techniques are validated to be advantageous in terms of improving the spectral efficiency and providing reliable connectivity, they are still unable to adequately address the problems of high energy consumption (EC) and high hardware/deployment cost (HDC). These problems will

Z. Xing and R. Wang are with the College of Electronics and Information Engineering, Tongji University, Shanghai 201804, China. R. Wang is also with the Shanghai Institute of Intelligent Science and Technology, Tongji University, Shanghai 201804, China (e-mail: zxing@tongji.edu.cn; ruiwang@tongji.edu.cn).

X. Yuan is with the National Key Laboratory of Science and Technology on Communications, University of Electronic Science and Technology of China, Chengdu, 610000, China (e-mail: xjyuan@uestc.edu.cn).

J. Wu is with the School of Computer Science, Fudan University, Shanghai 200433, China (e-mail: wujun@fudan.edu.cn).

become even more serious in the future sixth-generation (6G) wireless communication network.

Recently, the urgent demand for coping with the problems of high EC and HDC in 5G/6G, has promoted the emergence and development of a new concept, termed reconfigurable intelligent surface (RIS), which aims to make the wireless communication environment smarter and more controllable for combating the undesirable propagation conditions [2], [3]. An RIS is generally an artificial metasurface consisting of a large quantity of near-passive reflecting units, each of which is independently controlled in a software-defined manner to adjust the physical properties, such as phase shifts, of the impinging electromagnetic waves, so as to reflect the waves to a desired receiver [4]–[7]. As the RIS can generally be fabricated with low-cost simple electronic components (e.g. varactor diodes [8] and positive intrinsic-negative (PIN) diodes [9]) and does not need power-consuming radio-frequency (RF) chains to perform active signal retransmission, it has attracted considerable attention and has been envisioned as one of the most promising candidate technologies in 5G/6G [10].

Summarized from the existing researches, the RIS is mostly employed to assist the wireless communication or user localization when the line-of-sight (LoS) link is weak or even unavailable, and to improve the system performance including (but not limited to) channel capacity [11], physical-layer security [12], outage probability [13], robustness [14], spectral/energy efficiency [15]–[17], achievable data rate [18]–[20], potential positioning accuracy [21], [22], etc., under either perfect [11]–[16], [19]–[22] or non-ideal hardware conditions [17], [18]. To achieve these goals, the phase shift design/optimization, also known as passive beamforming, needs to be performed at the RIS. This implies that the RIS controller should first acquire adequate instantaneous channel state information (CSI) from the base station (BS). Although the instantaneous CSI can generally be obtained by various channel estimation techniques developed for the RIS-aided wireless communication [23]–[25], several problems still exist during this procedure. First, when the number of the RIS reflecting units is large, conventional CSI estimation techniques require a huge overhead for channel training. Second, when the BS acquires the CSI, the CSI needs to be delivered to the RIS controller via an additional link, which incurs an extra communication overhead [26]. Third, since the CSI is generally time-variant in real applications, the update of passive beamforming may become hysteretic due to training and/or communication delay, which seriously compromises the potential gain achieved by the use of RIS.

In view of the aforementioned issues, a novel RIS-aided

communication scheme based on user location information has been proposed recently [26]. Specifically, in the mmWave communication scenario, according to the spatial geometric relations between the coordinates of the BS, RIS, user and the array responses at each terminal side, the channel matrices or vectors can be directly reconstructed, based on which the transmit or passive beamforming can be optimized by using conventional methods. In practical applications, the positions of the BS and RIS are fixed and known after their deployments, while the position of a user can be easily acquired from the existing localization systems, e.g., the global positioning system (GPS) for outdoor users, or the ultra-wide band (UWB) for indoor users. Therefore, utilizing the location information to acquire the CSI can overcome the drawbacks of the conventional CSI estimation introduced in the previous paragraph.

However, the user position from the localization systems is generally inaccurate. Due to the unavoidable localization error caused by inherent accuracy limitation or hardware imperfection of the localization devices, the reconstructed channels suffer from CSI uncertainty. In such a situation, in order to maintain a good system performance, the transmit or passive beamforming should be designed robust to the CSI uncertainty. Up to now, there have already been several important prior works which studied the robust beamforming in the RIS-aided communication systems. For instance, G. Zhou, *et al.* [27], [28], considered both the bounded CSI error and the statistical CSI error, and designed robust transmit and passive beamforming optimization algorithms based on S-procedure and penalty convex-concave procedure (CCP); J. Zhang, *et al.* [29], and M. Zhao, *et al.* [30], focused on minimizing the average mean squared error (MSE) of the data symbols, or minimizing the transmit power with outage probability constraints, in consideration of the statistical CSI error. However, these works did not investigate the CSI error arising from the user location uncertainty, and might suffer from slow convergence when the number of transmit antennas or reflecting elements became large. To the best of our knowledge, how to achieve an efficient robust transmit and passive beamforming optimization approach based on the location information has not been explored yet, which motivates our research herein. Although in our previous conference paper [14], we addressed this remaining issue by relating the CSI error bound to the user location error bound and devising a worst-case robust beamforming optimization scheme based on saddle point theory, the proposed design in [14] was only suitable for a special far-field communication scenario, where the investigated BS-RIS and RIS-user channels contained simply LoS paths and the BS-RIS channel was rank-one. As such, in this work, we propose a novel worst-case robust beamforming optimization approach for the RIS-aided location information assisted wireless communication system, which applies to a more general communication scenario in the presence of ubiquitous Rician fading. In such a case, compared to [14], both the determination of the CSI error bound and the optimization process of the transmit and passive beamforming are considerably distinct and more challenging.

The contributions of this paper are summarized as follows.

- **Derivation of the CSI error bound:** First, a three-dimensional (3D) RIS-aided mmWave communication system is considered, where the locations of the BS, the RIS

and the user are adopted to acquire the CSI of the BS-RIS-user link. Under the assumption that the user location error is restricted in a spherical region [26], an approximate CSI error bound is derived by means of Taylor expansion, triangle inequality, power mean inequality, and semidefinite relaxation (SDR). The CSI error bound is empirically verified to be tight when the user location uncertainty is moderate, or when the user is far away from the RIS.

- **Robust transmit and passive beamforming:** After the CSI error bound is derived, a worst-case robust transmit and passive beamforming optimization problem is formulated. Since the original problem is non-convex and difficult to be solved efficiently, an iterative optimization approach is proposed to acquire a suboptimal solution. Specifically, in one iteration, the inner minimization is first completed to determine an optimal Lagrange dual variable, and the outer maximization is then accomplished to obtain an optimal phase-shift matrix. Owing to the unit-modulus characteristic of the reflectors, the subproblem of the outer maximization is converted into a constrained QCQP problem with the aid of matrix inversion lemma, and solved by the SDR when the phase shift arguments belong to $[0, 2\pi]$, or by the branch-and-bound (BnB) algorithm when the phase shift arguments are arbitrarily constrained.
- **Algorithm design and performance evaluation:** Based on the proposed iterative approach, the overall algorithm is finally built, and its computational complexity is analysed. Afterwards, the theoretical derivation of the CSI error bound is verified, and the performance of the developed algorithm is evaluated numerically. Compared with the conventional non-robust approach, the proposed algorithm shows strong robustness against the CSI uncertainty. Compared with the existing worst-case robust beamforming methods based on S-procedure and penalty CCP, our proposed approach performs better and converges faster in terms of the worst-case signal-to-noise ratio (SNR) at the receiver. Besides, our proposed algorithm with BnB has the advantages of being able to provide near-optimal solutions and deal with arbitrary phase shift argument sets.

The rest of this paper is organized as follows. Section II describes the system model and the problem formulation for the robust transmit and passive beamforming optimization. Section III derives the CSI error bound based on the user location error bound. Section IV proposes an iterative optimization approach to acquire the solutions of the transmit beamforming vector and the reflective phase-shift matrix. Section V carries out the simulations and comparisons to evaluate the performance of the proposed algorithm. Section VI draws the final conclusions and the prospects of the future work.

Notations: $[\mathbf{v}]_i$ and $[\mathbf{M}]_{(i,i)}$ represent the i -th and (i,i) -th element in vector \mathbf{v} and matrix \mathbf{M} . \mathbf{M}^T , \mathbf{M}^* and \mathbf{M}^H denote the transpose, conjugate and conjugate transpose of \mathbf{M} . $\mathbf{M} \in \mathbb{C}^{a \times b}$ means that \mathbf{M} is an $a \times b$ sized complex-value matrix. $\|\cdot\|_2$ symbolizes the ℓ_2 -norm. $\mathbb{E}\{\cdot\}$, $tr(\cdot)$ and $\arg\{\cdot\}$ denote the expectation, trace and argument, respectively. $\text{diag}(x_1, x_2, \dots, x_n)$ represents a diagonal matrix whose diagonal elements are (x_1, x_2, \dots, x_n) . $\Re\{x\}$ and $\Im\{x\}$ denote the real part and the imaginary part of x , respectively. $\mathbf{I}_{a \times a}$ is an $a \times a$ sized identity matrix.

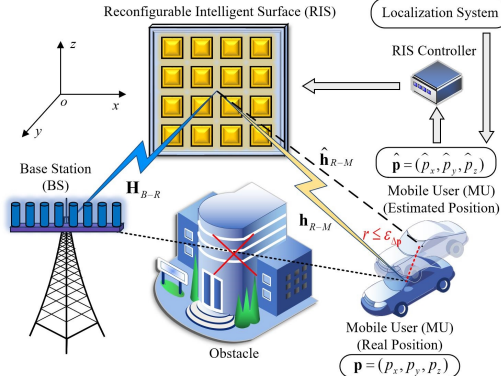


Fig. 1: The considered RIS-aided wireless communication system in a 3D propagation environment.

II. SYSTEM MODEL AND PROBLEM FORMULATION

In this paper, an RIS-aided mmWave communication system in a 3D propagation environment, as shown in Fig. 1, is investigated. The system is composed of a BS with a uniform linear array (ULA) consisting of M antennas, an RIS with a uniform square planar array (USPA) consisting of $L \times L = N$ reflecting elements with L being the number of rows or columns of the USPA, a mobile user (MU) with one antenna, and an RIS controller. The antenna spacing of the BS is d_{BS} , while the element spacing of the RIS is d_{RIS} . To guarantee a good communication performance, the RIS is deployed near the BS. For convenience of system description, a 3D Cartesian coordinate system, as shown in the top-left corner of Fig. 1, is established to specify the positions of the BS, the RIS and the MU. With the aid of coordinate indication, the position of the MU is represented by $\mathbf{p} = (p_x, p_y, p_z)^T$. Assume that the ULA on the BS and the USPA on the RIS are deployed parallel to the x -axis and the x - o - z plane, respectively. Then, let $\mathbf{q}_1 = (q_{x,1}, q_{y,1}, q_{z,1})^T$ denote the coordinates of the left-end BS antenna, and $\mathbf{v}_1 = (v_{x,1}, v_{y,1}, v_{z,1})^T$ denote the coordinates of the reflecting element in the bottom-left corner of the RIS. Hence, the positions of the i -th antenna on the BS, for $i = 1, 2, 3, \dots, M$, and the $(\ell + (k-1)L)$ -th reflecting element on the RIS, for $\ell = 1, 2, \dots, L$ and $k = 1, 2, \dots, L$, are represented by

$$\mathbf{q}_i = \mathbf{q}_1 + \boldsymbol{\delta}_{\mathbf{q}}(i), \quad (1)$$

$$\mathbf{v}_{\ell+(k-1)L} = \mathbf{v}_1 + \boldsymbol{\delta}_{\mathbf{v}}(\ell + (k-1)L), \quad (2)$$

where $\boldsymbol{\delta}_{\mathbf{q}}(i) = ((i-1)d_{BS}, 0, 0)^T$ and $\boldsymbol{\delta}_{\mathbf{v}}(\ell + (k-1)L) = ((\ell-1)d_{RIS}, 0, (k-1)d_{RIS})^T$.

Based on this system setup, the remainder of this section will illustrate the channel and received signal models, CSI error model, and problem formulation.

A. Channel and Received Signal Models

In this communication system, the direct path between the BS and the MU is assumed to be blocked. As the mmWave is sensitive to obstructions, only the BS-RIS-MU link is assumed available in this situation. For the BS-RIS-MU link, let $\mathbf{H}_{B-R} \in \mathbb{C}^{N \times M}$ and $\mathbf{h}_{R-M} \in \mathbb{C}^{N \times 1}$ denote the baseband equivalent

channels from BS to RIS and from RIS to MU, respectively, which are modelled as [16]

$$\mathbf{H}_{B-R} = \sqrt{\frac{\kappa_R}{1 + \kappa_R}} \mathbf{H}_{B-R}^{LoS} + \sqrt{\frac{1}{1 + \kappa_R}} \mathbf{H}_{B-R}^{NLoS}, \quad (3)$$

$$\mathbf{h}_{R-M} = \sqrt{\frac{\kappa_R}{1 + \kappa_R}} \mathbf{h}_{R-M}^{LoS} + \sqrt{\frac{1}{1 + \kappa_R}} \mathbf{h}_{R-M}^{NLoS}, \quad (4)$$

where κ_R denotes the Rician factor; $\mathbf{H}_{B-R}^{NLoS} \in \mathbb{C}^{N \times M}$ and $\mathbf{h}_{R-M}^{NLoS} \in \mathbb{C}^{N \times 1}$ are the non-LoS Rayleigh fading components, whose elements follow zero-mean complex Gaussian distributions [31]; $\mathbf{H}_{B-R}^{LoS} \in \mathbb{C}^{N \times M}$ and $\mathbf{h}_{R-M}^{LoS} \in \mathbb{C}^{N \times 1}$ are the LoS components given by (5) and (6) on the top of the next page [32], where λ is the signal wavelength; $\vartheta_{\ell+(k-1)L,i}$ and $\varpi_{\ell+(k-1)L}$, for $\ell = 1, 2, \dots, L$, $k = 1, 2, \dots, L$ and $i = 1, 2, \dots, M$, are expressed as

$$\vartheta_{\ell+(k-1)L,i} = \|\mathbf{v}_1 - \mathbf{q}_1\|_2 - \|\mathbf{v}_{\ell+(k-1)L} - \mathbf{q}_i\|_2, \quad (7)$$

$$\varpi_{\ell+(k-1)L} = \|\mathbf{v}_{\ell+(k-1)L} - \mathbf{p}\|_2 - \|\mathbf{v}_1 - \mathbf{p}\|_2. \quad (8)$$

$\rho_{Loss}^{B_i-R_{\ell+(k-1)L}}$ and $\rho_{Loss}^{R_{\ell+(k-1)L}-M}$ are, respectively, the large-scale path loss coefficients from the i -th BS antenna to the $(\ell + (k-1)L)$ -th RIS element and from the $(\ell + (k-1)L)$ -th RIS element to the MU, given by [16]

$$\rho_{Loss}^{B_i-R_{\ell+(k-1)L}} = \zeta_0 \left(\frac{d_{B_i-R_{\ell+(k-1)L}}}{d_0} \right)^{-\alpha}, \quad (9)$$

$$\rho_{Loss}^{R_{\ell+(k-1)L}-M} = \zeta_0 \left(\frac{d_{R_{\ell+(k-1)L}-M}}{d_0} \right)^{-\alpha}, \quad (10)$$

where d_0 is the reference distance; ζ_0 denotes the path loss at the reference distance of $d_0 = 1$ m; α represents the path loss exponent; $d_{B_i-R_{\ell+(k-1)L}}$ and $d_{R_{\ell+(k-1)L}-M}$ are given by

$$d_{B_i-R_{\ell+(k-1)L}} = \|\mathbf{v}_{\ell+(k-1)L} - \mathbf{q}_i\|_2,$$

$$d_{R_{\ell+(k-1)L}-M} = \|\mathbf{v}_{\ell+(k-1)L} - \mathbf{p}\|_2.$$

Based on the above channel models, the signal received by the MU is modelled as

$$y(t) = \sqrt{P_T} \mathbf{h}_{R-M}^H \Theta \mathbf{H}_{B-R} \mathbf{w} x(t) + n(t), \quad (11)$$

where P_T denotes the total transmit power; $x(t)$ represents the transmit symbol which satisfies $\mathbb{E}\{x^*(t)x(t)\} = 1$; $n(t) \sim \mathcal{CN}(0, \sigma_n^2)$ denotes the receiver noise; \mathbf{w} is the unit-norm transmit beamforming vector; Θ is the phase-shift matrix of the RIS, given by $\Theta = \text{diag}(\beta_1 e^{j\theta_1}, \beta_2 e^{j\theta_2}, \dots, \beta_N e^{j\theta_N})$, where $\beta_{\ell+(k-1)L}$ and $\theta_{\ell+(k-1)L}$ denote the amplitude and phase shift argument of the $(\ell + (k-1)L)$ -th reflecting element, respectively. As the RIS is a near-passive reflecting apparatus, we assume that the reflection amplitudes satisfy $\beta_1 = \beta_2 = \dots = \beta_N = 1$ [18] without loss of generality. The phase shift arguments belong to a set \mathcal{S} , where \mathcal{S} can be one of the following categories:

- 1) $\mathcal{S} = [0, 2\pi]$: the simplest and most universal argument set.
- 2) $\mathcal{S} = [\ell_l, \ell_u]$: a general argument set restricted within an arbitrary interval, where ℓ_l and ℓ_u are real values satisfying $\ell_l < \ell_u$.
- 3) $\mathcal{S} = \{0, \Delta\theta, \dots, (W_\theta - 1)\Delta\theta\}$: a discrete argument set with W_θ phase shift levels, where $\Delta\theta = 2\pi/W_\theta$ [17].

B. CSI Error Model

Considering that the locations of BS and RIS are stationary, the channel condition between BS and RIS hardly changes with

$$\mathbf{H}_{B-R}^{LoS} = \begin{pmatrix} \sqrt{\rho_{Loss}^{B_1-R_1}} e^{j \frac{2\pi}{\lambda} \vartheta_{1,1}} & \sqrt{\rho_{Loss}^{B_2-R_1}} e^{j \frac{2\pi}{\lambda} \vartheta_{1,2}} & \dots & \sqrt{\rho_{Loss}^{B_M-R_1}} e^{j \frac{2\pi}{\lambda} \vartheta_{1,M}} \\ \sqrt{\rho_{Loss}^{B_1-R_2}} e^{j \frac{2\pi}{\lambda} \vartheta_{2,1}} & \sqrt{\rho_{Loss}^{B_2-R_2}} e^{j \frac{2\pi}{\lambda} \vartheta_{2,2}} & \dots & \sqrt{\rho_{Loss}^{B_M-R_2}} e^{j \frac{2\pi}{\lambda} \vartheta_{2,M}} \\ \vdots & \vdots & \ddots & \vdots \\ \sqrt{\rho_{Loss}^{B_1-R_N}} e^{j \frac{2\pi}{\lambda} \vartheta_{N,1}} & \sqrt{\rho_{Loss}^{B_2-R_N}} e^{j \frac{2\pi}{\lambda} \vartheta_{N,2}} & \dots & \sqrt{\rho_{Loss}^{B_M-R_N}} e^{j \frac{2\pi}{\lambda} \vartheta_{N,M}} \end{pmatrix}, \quad (5)$$

$$\mathbf{h}_{R-M}^{LoS} = \left(\sqrt{\rho_{Loss}^{R_1-M}} e^{j \frac{2\pi}{\lambda} \varpi_1}, \sqrt{\rho_{Loss}^{R_2-M}} e^{j \frac{2\pi}{\lambda} \varpi_2}, \dots, \sqrt{\rho_{Loss}^{R_N-M}} e^{j \frac{2\pi}{\lambda} \varpi_N} \right)^T. \quad (6)$$

time. Moreover, because the RIS is close to the BS and the mmWave channel has limited scattering, the LoS component in the BS-RIS channel is dominant whereas the non-LoS component is substantially weak, resulting in $\mathbf{H}_{B-R} \approx \mathbf{H}_{B-R}^{LoS}$ [18], [33]. Therefore, by assuming that the exact locations of each antenna on the BS and each reflecting element on the RIS are fixed and known after their deployments, \mathbf{H}_{B-R} can be perfectly obtained by (5), (7) and (9). The location of the MU, provided by the existing localization systems, can be used to acquire \mathbf{h}_{R-M}^{LoS} based on (6), (8) and (10). However, the acquired RIS-MU channel contains an unavoidable error, which is primarily caused by the following two factors.

- **User location error:** In view of the inherent hardware imperfection, limited precision of measurements or some other unfavorable aspects, the user location obtained, e.g. from GPS or UWB, denoted by $\hat{\mathbf{p}} = (\hat{p}_x, \hat{p}_y, \hat{p}_z)^T$, is generally inaccurate. By referring to [26], $\hat{\mathbf{p}}$ satisfies $\mathbf{p} = \hat{\mathbf{p}} + \Delta\mathbf{p}$, where $\Delta\mathbf{p} = (\Delta p_x, \Delta p_y, \Delta p_z)^T$ is the user location error, bounded by $\|\Delta\mathbf{p}\|_2 = r \leq \epsilon_{\Delta\mathbf{p}}$, where $\epsilon_{\Delta\mathbf{p}}$ is a known small positive constant depending on the localization accuracy [26].
- **Non-LoS component:** Forasmuch as the mobility of the MU, the non-LoS Rayleigh fading component may not be neglected when the MU moves far away from the RIS. Although \mathbf{h}_{R-M}^{NLoS} is random, its ℓ_2 -norm within a certain communication duration can be determined by the existing channel norm feedback techniques based on pilot data sequence [34], [35] or on channel correlation matrix [36]. When the MU moves slowly, the ℓ_2 -norm of \mathbf{h}_{R-M}^{NLoS} can be regarded approximately as a fixed term in a short period, since the variation of channel condition between RIS and MU is slow. Thus, we can assume that $\|\mathbf{h}_{R-M}^{NLoS}\|_2$ is known and given by $\|\mathbf{h}_{R-M}^{NLoS}\|_2 = \delta_{R-M}^{NLoS}$.

Thus, the CSI error of the RIS-MU channel is defined by

$$\Delta\mathbf{h}_{R-M} = \mathbf{h}_{R-M} - \hat{\mathbf{h}}_{R-M} = \Delta\mathbf{h}_{R-M}^{LoS} + \Delta\mathbf{h}_{R-M}^{NLoS}, \quad (12)$$

where $\hat{\mathbf{h}}_{R-M}$ denotes the LoS part of RIS-MU channel acquired by $\hat{\mathbf{p}}$, which can be calculated via

$$\hat{\mathbf{h}}_{R-M} = \left(\sqrt{\hat{\rho}_{Loss}^{R_1-M}} e^{j \frac{2\pi}{\lambda} \hat{\varpi}_1}, \dots, \sqrt{\hat{\rho}_{Loss}^{R_N-M}} e^{j \frac{2\pi}{\lambda} \hat{\varpi}_N} \right)^T \quad (13)$$

where $\hat{\varpi}_{\ell+(k-1)L}$ is expressed as

$$\hat{\varpi}_{\ell+(k-1)L} = \|\mathbf{v}_{\ell+(k-1)L} - \hat{\mathbf{p}}\|_2 - \|\mathbf{v}_1 - \hat{\mathbf{p}}\|_2,$$

and $\hat{\rho}_{Loss}^{R_{\ell+(k-1)L}-M}$ is computed by (10) using

$$\hat{d}_{R_{\ell+(k-1)L}-M} = \|\mathbf{v}_{\ell+(k-1)L} - \hat{\mathbf{p}}\|_2.$$

As a result, $\Delta\mathbf{h}_{R-M}^{LoS}$, which represents the CSI error of the LoS component depending on $\Delta\mathbf{p}$, is given by

$$\Delta\mathbf{h}_{R-M}^{LoS} = \sqrt{\frac{\kappa_R}{1 + \kappa_R}} \mathbf{h}_{R-M}^{LoS} - \hat{\mathbf{h}}_{R-M}, \quad (14)$$

while $\Delta\mathbf{h}_{R-M}^{NLoS}$, which stands for the CSI error of the non-LoS component, is expressed as

$$\Delta\mathbf{h}_{R-M}^{NLoS} = \sqrt{\frac{1}{1 + \kappa_R}} \mathbf{h}_{R-M}^{NLoS}. \quad (15)$$

(14) and (15) indicate that in the mmWave communication with a large κ_R , $\Delta\mathbf{h}_{R-M}^{LoS}$ generally dominates the entire CSI error $\Delta\mathbf{h}_{R-M}$.

In the presence of $\Delta\mathbf{h}_{R-M}$, we aim to optimize \mathbf{w} and Θ based on \mathbf{h}_{R-M} and \mathbf{H}_{B-R} , by maximizing the worst-case SNR at the receiver.

C. Problem Formulation

For the aforementioned system model, the worst-case robust beamforming optimization problem is formulated as

$$\max_{\mathbf{w}, \Theta} \min_{\Delta\mathbf{h}_{R-M}} |(\hat{\mathbf{h}}_{R-M} + \Delta\mathbf{h}_{R-M})^H \Theta \mathbf{H}_{B-R} \mathbf{w}|^2, \quad (16a)$$

$$\text{s.t. } \|\mathbf{w}\|_2 = 1, \quad (16b)$$

$$\|\Delta\mathbf{h}_{R-M}\|_2 \leq \epsilon_{\Delta\mathbf{h}_{R-M}}, \quad (16c)$$

$$|\Theta|_{(i,i)} = 1, \quad i = 1, 2, \dots, N, \quad (16d)$$

$$\arg \{ |\Theta|_{(i,i)} \} \in \mathcal{S}, \quad i = 1, 2, \dots, N, \quad (16e)$$

where the constant terms of P_T and σ_n^2 are omitted for conciseness, without changing the optimization results. Constraint (16b) comes from the unit-norm transmit beamforming vector. Constraint (16c) means that the overall CSI error is bounded in a spherical uncertainty region. Constraint (16d) comes from the unit-modulus phase shifts of the RIS. Constraint (16e) represents the phase shift argument constraint.

It is noted that because the overall CSI error bound $\epsilon_{\Delta\mathbf{h}_{R-M}}$ in constraint (16c) is still undetermined here, it should first be derived on the basis of $\|\Delta\mathbf{p}\|_2 \leq \epsilon_{\Delta\mathbf{p}}$ and $\|\mathbf{h}_{R-M}^{NLoS}\|_2 = \delta_{R-M}^{NLoS}$ before solving problem (16). The derivation of $\epsilon_{\Delta\mathbf{h}_{R-M}}$ will be detailed in the next section.

III. DERIVATION OF THE CSI ERROR BOUND

This section is dedicated to the derivation of the overall CSI error bound in (16c) according to $\|\Delta\mathbf{p}\|_2 \leq \epsilon_{\Delta\mathbf{p}}$ and $\|\mathbf{h}_{R-M}^{NLoS}\|_2 = \delta_{R-M}^{NLoS}$. First, when retrospecting (12), we have (17) on the top of the next page, where ϵ_{R-M}^{LoS} denotes the upper bound of $\|\mathbf{h}_{R-M}^{LoS} - \hat{\mathbf{h}}_{R-M}\|_2$, which is unknown and should be derived according to $\|\Delta\mathbf{p}\|_2 \leq \epsilon_{\Delta\mathbf{p}}$.

A. Derivation of ϵ_{R-M}^{LoS}

Here we begin the derivation of ϵ_{R-M}^{LoS} from $\|\mathbf{h}_{R-M}^{LoS} - \hat{\mathbf{h}}_{R-M}\|_2$, which can be expanded into

$$\|\mathbf{h}_{R-M}^{LoS} - \hat{\mathbf{h}}_{R-M}\|_2 = \sqrt{\zeta_0 \left(\frac{1}{d_0} \right)^{-\alpha} \Omega(\Delta\mathbf{p})}, \quad (18)$$

$$\begin{aligned}
\|\Delta \mathbf{h}_{R-M}\|_2 &\leq \left\| \Delta \mathbf{h}_{R-M}^{LoS} \right\|_2 + \left\| \Delta \mathbf{h}_{R-M}^{NLoS} \right\|_2 = \left\| \sqrt{\frac{\kappa_R}{1+\kappa_R}} (\mathbf{h}_{R-M}^{LoS} - \hat{\mathbf{h}}_{R-M}) + \left(\sqrt{\frac{\kappa_R}{1+\kappa_R}} - 1 \right) \hat{\mathbf{h}}_{R-M} \right\|_2 + \sqrt{\frac{1}{1+\kappa_R}} \delta_{R-M}^{NLoS} \\
&\leq \sqrt{\frac{\kappa_R}{1+\kappa_R}} \left\| \mathbf{h}_{R-M}^{LoS} - \hat{\mathbf{h}}_{R-M} \right\|_2 + \left(1 - \sqrt{\frac{\kappa_R}{1+\kappa_R}} \right) \left\| \hat{\mathbf{h}}_{R-M} \right\|_2 + \sqrt{\frac{1}{1+\kappa_R}} \delta_{R-M}^{NLoS} \\
&\leq \sqrt{\frac{\kappa_R}{1+\kappa_R}} \epsilon_{R-M}^{LoS} + \left(1 - \sqrt{\frac{\kappa_R}{1+\kappa_R}} \right) \left\| \hat{\mathbf{h}}_{R-M} \right\|_2 + \sqrt{\frac{1}{1+\kappa_R}} \delta_{R-M}^{NLoS}.
\end{aligned} \tag{17}$$

where $\Omega(\Delta \mathbf{p})$ is a function of $\Delta \mathbf{p}$, expressed as (19) on the top of the next page, with $\mathfrak{U}_{\ell+(k-1)L}$ being detailed as

$$\begin{aligned}
\mathfrak{U}_{\ell+(k-1)L} &= \varpi_{\ell+(k-1)L} - \widehat{\varpi}_{\ell+(k-1)L} \\
&= (\|\mathbf{v}_{\ell+(k-1)L} - \hat{\mathbf{p}} - \Delta \mathbf{p}\|_2 - \|\mathbf{v}_1 - \hat{\mathbf{p}} - \Delta \mathbf{p}\|_2) \\
&\quad - (\|\mathbf{v}_{\ell+(k-1)L} - \hat{\mathbf{p}}\|_2 - \|\mathbf{v}_1 - \hat{\mathbf{p}}\|_2) \\
&\stackrel{(a)}{\approx} \left(\frac{(\mathbf{v}_1 - \hat{\mathbf{p}})^T}{\|\mathbf{v}_1 - \hat{\mathbf{p}}\|_2} - \frac{(\mathbf{v}_{\ell+(k-1)L} - \hat{\mathbf{p}})^T}{\|\mathbf{v}_{\ell+(k-1)L} - \hat{\mathbf{p}}\|_2} \right) \Delta \mathbf{p} \\
&= \boldsymbol{\eta}_{\ell+(k-1)L}^T \Delta \mathbf{p},
\end{aligned}$$

where $\boldsymbol{\eta}_{\ell+(k-1)L} = \left(\frac{\mathbf{v}_1 - \hat{\mathbf{p}}}{\|\mathbf{v}_1 - \hat{\mathbf{p}}\|_2} - \frac{\mathbf{v}_{\ell+(k-1)L} - \hat{\mathbf{p}}}{\|\mathbf{v}_{\ell+(k-1)L} - \hat{\mathbf{p}}\|_2} \right)$ is independent of $\Delta \mathbf{p}$; derivation (a) uses the property that for a fixed real-valued vector \mathbf{b} and a variable \mathbf{x} , $\|\mathbf{b} - \mathbf{x}\|_2$ can be well approximated by its first-order approximation of $\|\mathbf{b} - \mathbf{x}\|_2 \approx \|\mathbf{b}\|_2 + \langle \nabla_{\mathbf{x}=\mathbf{0}} \|\mathbf{b} - \mathbf{x}\|_2, \mathbf{x} \rangle = \|\mathbf{b}\|_2 - \frac{\mathbf{b}^T}{\|\mathbf{b}\|_2} \mathbf{x}$.

It is remarkable that when $\mathbf{v}_{\ell+(k-1)L}$ and $\hat{\mathbf{p}}$ are given, deriving ϵ_{R-M}^{LoS} is equivalent to deriving the maximum of $\Omega(\Delta \mathbf{p})$ under the constraint of $\|\Delta \mathbf{p}\|_2 \leq \epsilon_{\Delta \mathbf{p}}$, which however, is a challenging task, as $\Delta \mathbf{p}$ appears in both the cosine function and the ℓ_2 -norm. In view of this issue, we will further transform $\Omega(\Delta \mathbf{p})$ into a simpler form by means of approximation.

Nevertheless, the approximation of $\Omega(\Delta \mathbf{p})$ may lead to an inaccurate ϵ_{R-M}^{LoS} , implying that the theoretically derived ϵ_{R-M}^{LoS} will be either higher or lower than the practical ϵ_{R-M}^{LoS} . Both of the two outcomes will influence the optimal solution of problem (16) to some extent. Fortunately, if the theoretically derived ϵ_{R-M}^{LoS} is higher than the practical ϵ_{R-M}^{LoS} , the worst-case CSI experienced during the optimization process will become even worse than the practical worst-case CSI, hence resulting in a more robust solution for problem (16). Consequently, in order to preserve the robustness of the transmit and passive beamforming, we need to derive an approximate *upper bound* of the maximum of $\Omega(\Delta \mathbf{p})$ under $\|\Delta \mathbf{p}\|_2 \leq \epsilon_{\Delta \mathbf{p}}$. The result is provided in the following Lemma 1.

Lemma 1. When $\|\Delta \mathbf{p}\|_2 \leq \epsilon_{\Delta \mathbf{p}}$, the approximate upper bound of the maximum of $\Omega(\Delta \mathbf{p})$, denoted by $\Omega_{\max}^{\text{Upp}}$, can be derived as

$$\Omega_{\max}^{\text{Upp}} = \max_{\mathbf{P} \succeq \mathbf{0}} \left\{ -\frac{4\pi^4}{3\lambda^4 N} \text{tr}^2(\mathbf{SP}) + \text{tr}(\mathbf{RP}) \right\} \tag{20}$$

from the solution of the following convex problem:

$$\max_{\mathbf{P} \succeq \mathbf{0}} -\frac{4\pi^4}{3\lambda^4 N} \text{tr}^2(\mathbf{SP}) + \text{tr}(\mathbf{RP}), \tag{21a}$$

$$\text{s.t. } \text{tr}(\mathbf{P}) \leq \epsilon_{\Delta \mathbf{p}}^2, \tag{21b}$$

where \mathbf{S} and \mathbf{R} are expressed as

$$\begin{aligned}
\mathbf{S} &= \sum_{k=1}^L \sum_{\ell=1}^L \left\{ (\|\mathbf{v}_{\ell+(k-1)L} - \hat{\mathbf{p}}\|_2 - \epsilon_{\Delta \mathbf{p}})^{-\frac{\alpha}{4}} \right. \\
&\quad \times \left. \|\mathbf{v}_{\ell+(k-1)L} - \hat{\mathbf{p}}\|_2^{-\frac{\alpha}{4}} \boldsymbol{\Xi}_{\ell+(k-1)L} \right\}, \tag{22}
\end{aligned}$$

$$\begin{aligned}
\mathbf{R} &= \sum_{k=1}^L \sum_{\ell=1}^L \left\{ \frac{1}{2} \mathbf{G}_\alpha - \left\| \mathbf{v}_{\ell+(k-1)L} - \hat{\mathbf{p}} \right\|_2^{-\frac{\alpha}{2}} \mathbf{G}_{\frac{\alpha}{2}} \right. \\
&\quad + \frac{4\pi^2}{\lambda^2} \left(\left\| \mathbf{v}_{\ell+(k-1)L} - \hat{\mathbf{p}} \right\|_2 - \epsilon_{\Delta \mathbf{p}} \right)^{-\frac{\alpha}{2}} \\
&\quad \times \left. \left\| \mathbf{v}_{\ell+(k-1)L} - \hat{\mathbf{p}} \right\|_2^{-\frac{\alpha}{2}} \boldsymbol{\Xi}_{\ell+(k-1)L} \right\}, \tag{23}
\end{aligned}$$

in which \mathbf{G}_α , $\mathbf{G}_{\frac{\alpha}{2}}$ and $\boldsymbol{\Xi}_{\ell+(k-1)L}$ are given by

$$\begin{aligned}
\mathbf{G}_\alpha &= \alpha(\alpha+2) \left\| \mathbf{v}_{\ell+(k-1)L} - \hat{\mathbf{p}} \right\|_2^{-\alpha-4} \\
&\quad \times (\hat{\mathbf{p}} - \mathbf{v}_{\ell+(k-1)L}) (\hat{\mathbf{p}} - \mathbf{v}_{\ell+(k-1)L})^T \\
&\quad - \alpha \left\| \mathbf{v}_{\ell+(k-1)L} - \hat{\mathbf{p}} \right\|_2^{-\alpha-2} \mathbf{I}_{3 \times 3}, \tag{24}
\end{aligned}$$

$$\begin{aligned}
\mathbf{G}_{\frac{\alpha}{2}} &= \frac{\alpha}{2} \left(\frac{\alpha}{2} + 2 \right) \left\| \mathbf{v}_{\ell+(k-1)L} - \hat{\mathbf{p}} \right\|_2^{-\frac{\alpha}{2}-4} \\
&\quad \times (\hat{\mathbf{p}} - \mathbf{v}_{\ell+(k-1)L}) (\hat{\mathbf{p}} - \mathbf{v}_{\ell+(k-1)L})^T \\
&\quad - \frac{\alpha}{2} \left\| \mathbf{v}_{\ell+(k-1)L} - \hat{\mathbf{p}} \right\|_2^{-\frac{\alpha}{2}-2} \mathbf{I}_{3 \times 3}, \tag{25}
\end{aligned}$$

$$\boldsymbol{\Xi}_{\ell+(k-1)L} = \boldsymbol{\eta}_{\ell+(k-1)L} \boldsymbol{\eta}_{\ell+(k-1)L}^T. \tag{26}$$

Proof. The proof is given in Appendix A. \square

After obtaining $\Omega_{\max}^{\text{Upp}}$ from (20), according to (18), we have

$$\epsilon_{R-M}^{LoS} \approx \sqrt{\zeta_0 \left(\frac{1}{d_0} \right)^{-\alpha}} \Omega_{\max}^{\text{Upp}}. \tag{27}$$

B. Determination of $\epsilon_{\Delta \mathbf{h}_{R-M}}$

After deriving ϵ_{R-M}^{LoS} , based on (17), we consequently obtain

$$\begin{aligned}
\epsilon_{\Delta \mathbf{h}_{R-M}} &= \sqrt{\frac{\kappa_R}{1+\kappa_R}} \epsilon_{R-M}^{LoS} + \left(1 - \sqrt{\frac{\kappa_R}{1+\kappa_R}} \right) \left\| \hat{\mathbf{h}}_{R-M} \right\|_2 \\
&\quad + \sqrt{\frac{1}{1+\kappa_R}} \delta_{R-M}^{NLoS}, \tag{28}
\end{aligned}$$

which completes the derivation of the CSI error bound.

IV. ROBUST TRANSMIT AND PASSIVE BEAMFORMING

Since $\epsilon_{\Delta \mathbf{h}_{R-M}}$ has been derived and the constraint of (16c) has been determined, we are now ready to solve problem (16), by proposing a robust beamforming optimization approach using the CSI acquired completely from the location information.

According to (16a) and (16b), the optimal transmit beamforming vector, denoted by $\bar{\mathbf{w}}$, is readily formed by

$$\bar{\mathbf{w}} = \frac{\mathbf{H}_{B-R}^H \boldsymbol{\Theta}^H (\hat{\mathbf{h}}_{R-M} + \Delta \mathbf{h}_{R-M})}{\|(\hat{\mathbf{h}}_{R-M} + \Delta \mathbf{h}_{R-M})^H \boldsymbol{\Theta} \mathbf{H}_{B-R}\|_2}. \tag{29}$$

Note that in (29), $\boldsymbol{\Theta}$ and $\Delta \mathbf{h}_{R-M}$ are both variables to be optimized. Thus, in order to settle $\bar{\mathbf{w}}$, the optimal $\boldsymbol{\Theta}$ and $\Delta \mathbf{h}_{R-M}$ should be determined first.

By substituting (29) into (16a) and (16b), problem (16) is recast as

$$\Omega(\Delta\mathbf{p}) = \sum_{k=1}^L \sum_{\ell=1}^L \left\{ \|\mathbf{v}_{\ell+(k-1)L} - \hat{\mathbf{p}} - \Delta\mathbf{p}\|_2^{-\alpha} + \|\mathbf{v}_{\ell+(k-1)L} - \hat{\mathbf{p}}\|_2^{-\alpha} \right\} - 2 \sum_{k=1}^L \sum_{\ell=1}^L \left\{ \|\mathbf{v}_{\ell+(k-1)L} - \hat{\mathbf{p}} - \Delta\mathbf{p}\|_2^{-\frac{\alpha}{2}} \|\mathbf{v}_{\ell+(k-1)L} - \hat{\mathbf{p}}\|_2^{-\frac{\alpha}{2}} \cos\left(\frac{2\pi}{\lambda} \mathbf{u}_{\ell+(k-1)L}\right) \right\}. \quad (19)$$

$$\max_{\Theta} \min_{\Delta\mathbf{h}_{R-M}} \|\hat{\mathbf{h}}_{R-M} + \Delta\mathbf{h}_{R-M}\|^H \Theta \mathbf{H}_{B-R} \|^2, \quad (30a)$$

$$\text{s.t. } \|\Delta\mathbf{h}_{R-M}\|_2 \leq \epsilon_{\Delta\mathbf{h}_{R-M}}, \quad (30b)$$

$$|[\Theta]_{(i,i)}| = 1, \quad i = 1, 2, \dots, N, \quad (30c)$$

$$\arg\{[\Theta]_{(i,i)}\} \in \mathcal{S}, \quad i = 1, 2, \dots, N, \quad (30d)$$

which is a max-min problem with respect to Θ and $\Delta\mathbf{h}_{R-M}$. To solve a max-min problem, existing methods such as S-procedure [37] or saddle point theory [38] based techniques, can be applied to eliminate the disturbance caused by the nondeterminacy of the CSI error, or to find the worst-case CSI from an equivalent min-max problem. However, in view of 1) the existence of the unit-modulus constraint in (30c) and the argument constraint in (30d), and 2) the difficulty in determining the closed-form optimal Θ , using these conventional methods to solve problem (30) is a hard nut to crack. Therefore, in this section, we develop an iterative optimization approach to solve problem (30), and design the overall optimization algorithm.

A. Proposed Iterative Optimization Approach

This subsection focuses on finding the solution of problem (30), by iteratively solving the inner minimization problem and the outer maximization problem. In particular, unlike the existing iterative algorithms in e.g. [27] or [28] which provide approximate solutions of the subproblems in each iteration, here we propose a novel iterative optimization approach through the instrumentality of Lagrange multiplier and matrix inverse lemma. In our approach, the solution of each subproblem is theoretically optimal, so that our algorithm can perform better and converge much more quickly to the optimum without many iterations.

1) Solve the Inner Minimization Problem:

To solve problem (30), let us first consider the following inner minimization problem when Θ is given:

$$\min_{\Delta\mathbf{h}_{R-M}} \|\hat{\mathbf{h}}_{R-M} + \Delta\mathbf{h}_{R-M}\|^H \Theta \mathbf{H}_{B-R} \|^2, \quad (31a)$$

$$\text{s.t. } \|\Delta\mathbf{h}_{R-M}\|_2 \leq \epsilon_{\Delta\mathbf{h}_{R-M}}. \quad (31b)$$

Here, we can rewrite constraint (31b) as

$$\Delta\mathbf{h}_{R-M}^H \Delta\mathbf{h}_{R-M} - \epsilon_{\Delta\mathbf{h}_{R-M}}^2 \leq 0, \quad (32)$$

so that problem (31) is a standard QCQP problem with respect to $\Delta\mathbf{h}_{R-M}$. To acquire the optimal solution of $\Delta\mathbf{h}_{R-M}$, we construct the Lagrange function:

$$\begin{aligned} \mathcal{L}(\Delta\mathbf{h}_{R-M}, \mu) &= \|\hat{\mathbf{h}}_{R-M} + \Delta\mathbf{h}_{R-M}\|^H \Theta \mathbf{H}_{B-R} \|^2 \\ &\quad + \mu \left(\Delta\mathbf{h}_{R-M}^H \Delta\mathbf{h}_{R-M} - \epsilon_{\Delta\mathbf{h}_{R-M}}^2 \right) \\ &= \Delta\mathbf{h}_{R-M}^H (\Theta \mathbf{H}_{B-R} \mathbf{H}_{B-R}^H \Theta^H + \mu \mathbf{I}) \Delta\mathbf{h}_{R-M} \\ &\quad + 2\Re \left\{ \hat{\mathbf{h}}_{R-M}^H \Theta \mathbf{H}_{B-R} \mathbf{H}_{B-R}^H \Theta^H \Delta\mathbf{h}_{R-M} \right\} \\ &\quad + \hat{\mathbf{h}}_{R-M}^H \Theta \mathbf{H}_{B-R} \mathbf{H}_{B-R}^H \Theta^H \hat{\mathbf{h}}_{R-M} - \mu \epsilon_{\Delta\mathbf{h}_{R-M}}^2, \end{aligned} \quad (33)$$

where μ is the Lagrange dual variable.

The optimal solutions of μ and $\Delta\mathbf{h}_{R-M}$ should satisfy the Karush-Kuhn-Tucker (KKT) conditions, listed as

$$\frac{\partial \mathcal{L}(\Delta\mathbf{h}_{R-M}, \mu)}{\partial \Delta\mathbf{h}_{R-M}} = \mathbf{0}, \quad (34a)$$

$$\Delta\mathbf{h}_{R-M}^H \Delta\mathbf{h}_{R-M} - \epsilon_{\Delta\mathbf{h}_{R-M}}^2 \leq 0, \quad (34b)$$

$$\mu \geq 0, \quad (34c)$$

$$\mu \left(\Delta\mathbf{h}_{R-M}^H \Delta\mathbf{h}_{R-M} - \epsilon_{\Delta\mathbf{h}_{R-M}}^2 \right) = 0. \quad (34d)$$

By calculating $\frac{\partial \mathcal{L}(\Delta\mathbf{h}_{R-M}, \mu)}{\partial \Delta\mathbf{h}_{R-M}} = \mathbf{0}$, we obtain

$$\begin{aligned} &(\Theta \mathbf{H}_{B-R} \mathbf{H}_{B-R}^H \Theta^H + \mu \mathbf{I})^T \Delta\mathbf{h}_{R-M}^* \\ &+ (\Theta \mathbf{H}_{B-R} \mathbf{H}_{B-R}^H \Theta^H \hat{\mathbf{h}}_{R-M})^* = \mathbf{0}, \end{aligned} \quad (35)$$

from which we derive the closed-form worst-case $\Delta\mathbf{h}_{R-M}$ with respect to μ and Θ , denoted by $\overline{\Delta\mathbf{h}}_{R-M}(\mu, \Theta)$, as

$$\begin{aligned} \overline{\Delta\mathbf{h}}_{R-M}(\mu, \Theta) &= -(\Theta \mathbf{H}_{B-R} \mathbf{H}_{B-R}^H \Theta^H + \mu \mathbf{I})^{-1} \\ &\times \Theta \mathbf{H}_{B-R} \mathbf{H}_{B-R}^H \Theta^H \hat{\mathbf{h}}_{R-M}. \end{aligned} \quad (36)$$

According to (34d), the optimal solutions of $\Delta\mathbf{h}_{R-M}$ and μ should either satisfy $\mu = 0$ or $\Delta\mathbf{h}_{R-M}^H \Delta\mathbf{h}_{R-M} - \epsilon_{\Delta\mathbf{h}_{R-M}}^2 = 0$. If $\mu = 0$, $\overline{\Delta\mathbf{h}}_{R-M}(\mu, \Theta)$ in (36) degenerates into $\overline{\Delta\mathbf{h}}_{R-M}(\mu, \Theta) = \overline{\Delta\mathbf{h}}_{R-M}(0, \Theta) = -\hat{\mathbf{h}}_{R-M}$, which makes the objective function in (31a) reduce to zero. In this case, the optimization process fails to find an optimal Θ . Therefore, the optimization process is feasible only if $\mu > 0$ and $\Delta\mathbf{h}_{R-M}^H \Delta\mathbf{h}_{R-M} - \epsilon_{\Delta\mathbf{h}_{R-M}}^2 = 0$.

By substituting $\overline{\Delta\mathbf{h}}_{R-M}(\mu, \Theta)$ in (36) into $\Delta\mathbf{h}_{R-M}^H \Delta\mathbf{h}_{R-M} = \epsilon_{\Delta\mathbf{h}_{R-M}}^2$, we obtain (37) on the top of the next page, where the solution of μ , denoted by $\overline{\mu}$, can be found by using the well-known bisection method [43].

After $\overline{\mu}$ is obtained, $\overline{\Delta\mathbf{h}}_{R-M}(\mu, \Theta)$ in (36) can be recast as $\overline{\Delta\mathbf{h}}_{R-M}(\overline{\mu}, \Theta)$. By substituting $\overline{\Delta\mathbf{h}}_{R-M}(\overline{\mu}, \Theta)$ into problem (30), we obtain the outer maximization of

$$\max_{\Theta} \mathcal{F}(\Theta), \quad (38a)$$

$$\text{s.t. } \mathcal{C}(\Theta) \leq 0, \quad (38b)$$

$$|[\Theta]_{(i,i)}| = 1, \quad i = 1, 2, \dots, N, \quad (38c)$$

$$\arg\{[\Theta]_{(i,i)}\} \in \mathcal{S}, \quad i = 1, 2, \dots, N, \quad (38d)$$

where $\mathcal{F}(\Theta)$ and $\mathcal{C}(\Theta)$ are, respectively, specified in (39) and (40) on the top of the next page.

2) Solve the Outer Maximization Problem:

Subsequently, we focus on solving problem (38). It is notable that problem (38) is a complicated non-convex problem containing the inverse of $\Theta \mathbf{H}_{B-R} \mathbf{H}_{B-R}^H \Theta^H + \overline{\mu} \mathbf{I}$, which makes problem (38) difficult to be solved efficiently. To deal with $(\Theta \mathbf{H}_{B-R} \mathbf{H}_{B-R}^H \Theta^H + \overline{\mu} \mathbf{I})^{-1}$, one feasible choice is to define a new variable as $\mathbf{Q} = (\Theta \mathbf{H}_{B-R} \mathbf{H}_{B-R}^H \Theta^H + \overline{\mu} \mathbf{I})^{-1}$, and optimize Θ and \mathbf{Q} iteratively until the optimization process converges [42]. However, this choice has one major drawback, i.e. additional iterations are included in the optimization process, leading to an increase of the overall computational complexity. In view of this defect, we focus on pursuing another effective

$$\hat{\mathbf{h}}_{R-M}^H \Theta \mathbf{H}_{B-R} \mathbf{H}_{B-R}^H \Theta^H \left(\Theta \mathbf{H}_{B-R} \mathbf{H}_{B-R}^H \Theta^H + \mu \mathbf{I} \right)^{-2} \Theta \mathbf{H}_{B-R} \mathbf{H}_{B-R}^H \Theta^H \hat{\mathbf{h}}_{R-M} - \epsilon_{\Delta \mathbf{h}_{R-M}}^2 = 0. \quad (37)$$

$$\mathcal{F}(\Theta) = \left\| \left[\hat{\mathbf{h}}_{R-M} - \left(\Theta \mathbf{H}_{B-R} \mathbf{H}_{B-R}^H \Theta^H + \bar{\mu} \mathbf{I} \right)^{-1} \Theta \mathbf{H}_{B-R} \mathbf{H}_{B-R}^H \Theta^H \hat{\mathbf{h}}_{R-M} \right]^H \Theta \mathbf{H}_{B-R} \right\|_2^2, \quad (39)$$

$$\mathcal{C}(\Theta) = \left[\left(\Theta \mathbf{H}_{B-R} \mathbf{H}_{B-R}^H \Theta^H + \bar{\mu} \mathbf{I} \right)^{-1} \Theta \mathbf{H}_{B-R} \mathbf{H}_{B-R}^H \Theta^H \hat{\mathbf{h}}_{R-M} \right]^H \left[\left(\Theta \mathbf{H}_{B-R} \mathbf{H}_{B-R}^H \Theta^H + \bar{\mu} \mathbf{I} \right)^{-1} \Theta \mathbf{H}_{B-R} \mathbf{H}_{B-R}^H \Theta^H \hat{\mathbf{h}}_{R-M} \right] - \epsilon_{\Delta \mathbf{h}_{R-M}}^2. \quad (40)$$

way to simplify the objective function and the constraints by adopting matrix inverse lemma in the following Proposition 1.

Proposition 1. *With the aid of the matrix inverse lemma, problem (38) can be transformed into a QCQP problem with argument and unit-modulus constraints, specifically given by*

$$\max_{\Theta} \Theta^T \text{diag}\{\hat{\mathbf{h}}_{R-M}^H\} \mathbf{Y} \mathbf{Y}^H \text{diag}\{\hat{\mathbf{h}}_{R-M}\} \Theta^*, \quad (41a)$$

$$\text{s.t. } \Theta^T \text{diag}\{\hat{\mathbf{h}}_{R-M}^H\} \mathbf{X} \text{diag}\{\hat{\mathbf{h}}_{R-M}\} \Theta^* \leq \epsilon_{\Delta \mathbf{h}_{R-M}}^2, \quad (41b)$$

$$|[\Theta]_i| = 1, \quad i = 1, 2, \dots, N, \quad (41c)$$

$$\arg\{[\Theta]_i\} \in \mathcal{S}, \quad i = 1, 2, \dots, N, \quad (41d)$$

where $\Theta = (e^{j\theta_1}, e^{j\theta_2}, \dots, e^{j\theta_N})^T$ is a column vector containing the diagonal elements of Θ ; \mathbf{Y} and \mathbf{X} are given in (61) and (63) in Appendix B, which are independent of Θ .

Proof. The proof is given in Appendix B. \square

Problem (41) can be solved by various existing techniques. Here, we briefly introduce two state-of-the-art algorithms for solving problem (41), which are semidefinite relaxation (SDR) algorithm and branch-and-bound (BnB) algorithm. In specific, the BnB is slightly modified to deal with our problem.

1) **SDR algorithm:** When $\mathcal{S} = [0, 2\pi]$, problem (41) can be solved by the SDR algorithm, which has been widely utilized in wireless communication and signal processing fields to transform non-convex problems into semidefinite programming (SDP) problems. Considering problem (41) as an example, the main idea of SDR is to introduce a new variable $\mathbf{C} = \Theta^* \Theta^T$, and then transform problem (41) by dropping the rank-one constraint into

$$\max_{\mathbf{C} \succeq 0} \text{tr} \left(\text{diag}\{\hat{\mathbf{h}}_{R-M}^H\} \mathbf{Y} \mathbf{Y}^H \text{diag}\{\hat{\mathbf{h}}_{R-M}\} \mathbf{C} \right), \quad (42a)$$

$$\text{s.t. } \text{tr} \left(\text{diag}\{\hat{\mathbf{h}}_{R-M}^H\} \mathbf{X} \text{diag}\{\hat{\mathbf{h}}_{R-M}\} \mathbf{C} \right) \leq \epsilon_{\Delta \mathbf{h}_{R-M}}^2, \quad (42b)$$

$$\text{tr}(\mathbf{E}_i \mathbf{C}) = 1, \quad i = 1, 2, \dots, N. \quad (42c)$$

where the matrix \mathbf{E}_i satisfies

$$[\mathbf{E}_i]_{(m,n)} = \begin{cases} 1, & m = n = i; \\ 0, & \text{otherwise.} \end{cases} \quad (43)$$

Problem (42) can be solved by existing methods such as interior-point method. To address the omitted rank-one constraint after solving problem (42) and obtaining the solution of \mathbf{C} , denoted by $\bar{\mathbf{C}}$, one can perform eigenvalue decomposition for $\bar{\mathbf{C}}$ to acquire the optimal Θ if $\bar{\mathbf{C}}$ is rank-one, or use the Gaussian randomization to acquire an approximate solution of Θ if $\bar{\mathbf{C}}$ is not rank-one [39]. Nevertheless, $\bar{\mathbf{C}}$ is generally not rank-one when the problem dimension is high, so that a non-zero gap between $\bar{\mathbf{C}}$ and the true optimal \mathbf{C} exists in most cases. In addition, if \mathcal{S} is an arbitrary argument set of $\mathcal{S} = [\ell_l, \ell_u]$ instead of $\mathcal{S} = [0, 2\pi]$, the SDR fails to solve problem (41). Forasmuch as these drawbacks of the SDR, the BnB has been proposed, with the details stated below.

2) **BnB algorithm:** The BnB algorithm was proposed in [40], [41] to find the global optimal solution of complex quadratic programming problems, by branching on the argument sets. Compared with the SDR, the BnB has two major advantages. First, the BnB can deal with arbitrary argument sets of $\mathcal{S} = [\ell_l, \ell_u]$ with $\ell_u - \ell_l \leq \pi$, such as $\mathcal{S} = [0, \pi]$, $\mathcal{S} = [0, \frac{\pi}{2}]$, or discrete argument values, whereas the SDR is only able to handle $\mathcal{S} = [0, 2\pi]$. Second, the solution of BnB can be very close to the true optimum after sufficient times of iterations.

Since the BnB requires $\ell_u - \ell_l \leq \pi$, when dealing with $\mathcal{S} = [\ell_l, \ell_u]$ in which $\ell_u - \ell_l > \pi$, we first divide \mathcal{S} into two subsets of $\mathcal{S}_1 = [\ell_l, \ell_m]$ and $\mathcal{S}_2 = [\ell_m, \ell_u]$, where $\mathcal{S}_1 + \mathcal{S}_2 = \mathcal{S}$ and $\ell_m - \ell_l = \pi$ ¹. For each subset, we construct a convex envelope, denoted by $\mathcal{E}_i = \{[\Theta]_i | \Re\{a_i^*[\Theta]_i\} \geq \cos \frac{\ell_{\text{right}} - \ell_{\text{left}}}{2}\}$, where $a_i = \cos \frac{\ell_{\text{right}} + \ell_{\text{left}}}{2} + j \sin \frac{\ell_{\text{right}} + \ell_{\text{left}}}{2}$; ℓ_{left} and ℓ_{right} satisfy $\ell_{\text{left}} = \ell_l$ and $\ell_{\text{right}} = \ell_m$ for subset \mathcal{S}_1 , or satisfy $\ell_{\text{left}} = \ell_m$ and $\ell_{\text{right}} = \ell_u$ for subset \mathcal{S}_2 . For more visual details, one can refer to [Fig. 1, 40] which depicts the convex envelope. Then, based on \mathcal{E}_i , we reformulate problem (41) as

$$\max_{\mathbf{C} \succeq 0, \Theta} \text{tr} \left(\text{diag}\{\hat{\mathbf{h}}_{R-M}^H\} \mathbf{Y} \mathbf{Y}^H \text{diag}\{\hat{\mathbf{h}}_{R-M}\} \mathbf{C} \right), \quad (44a)$$

$$\text{s.t. } (42b), \quad (42c), \quad (44b)$$

$$[\Theta]_i \in \mathcal{E}_i, \quad i = 1, 2, \dots, N, \quad (44c)$$

$$\mathbf{C} \succeq \Theta^* \Theta^T. \quad (44d)$$

which is convex. Afterwards, considering problem (44), we adopt [Algorithm 1, 40] to find the optimal solutions for the two subsets of \mathcal{S}_1 and \mathcal{S}_2 separately, which are represented by $\bar{\Theta}_{\mathcal{S}_1}$ and $\bar{\Theta}_{\mathcal{S}_2}$. The main idea of [Algorithm 1, 40] is to continuously execute the following procedure:

1) Cut \mathcal{S}_1 or \mathcal{S}_2 into smaller sets and solve problem (44).

2) Use the rounding operation to acquire a projection of the solution of Θ on the feasible domain of $[\Theta]_i = 1$.

The procedure stops when the gap between the objective values with respect to the projection and the solution of problem (44) is smaller than a predetermined error tolerance ϵ_{BnB} . After obtaining $\bar{\Theta}_{\mathcal{S}_1}$ and $\bar{\Theta}_{\mathcal{S}_2}$, we substitute them into (41a) to calculate the objective values. Then, from $\bar{\Theta}_{\mathcal{S}_1}$ and $\bar{\Theta}_{\mathcal{S}_2}$, we choose the one corresponding to the higher objective value as the final solution. The flowchart of the modified BnB in our algorithm is described in Fig. 2, which shows the above process.

Moreover, when dealing with the discrete phase shift argument sets, the BnB algorithm in [40] can be readily adopted by constructing a polyhedral convex hull. One can refer to [40] for more details.

Based on the analysis in this subsection, the overall robust beamforming optimization algorithm is designed as follows.

¹For example, if $\mathcal{S} = [\ell_l, \ell_u] = [0, 2\pi]$, we divide \mathcal{S} into $\mathcal{S}_1 = [0, \pi]$ and $\mathcal{S}_2 = [\pi, 2\pi]$, with $\ell_l = 0$, $\ell_m = \pi$ and $\ell_u = 2\pi$.

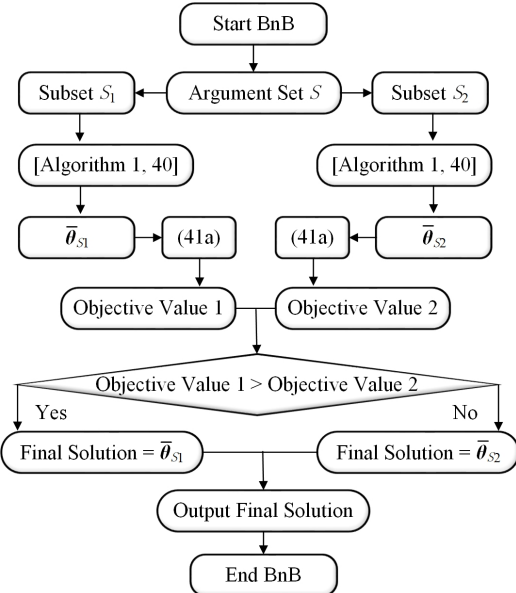


Fig. 2: The flowchart of the BnB in our algorithm.

B. Overall Algorithm Design

Our robust beamforming optimization algorithm is designed as **Algorithm 1**, which can be summarized as 4 steps.

- **Step 1: Input parameters:** the parameters including locations, number of antennas and reflecting elements, etc., are input to the algorithm.
- **Step 2: Compute CSI error bound:** the CSI error bound $\epsilon_{\Delta h_{R-M}}$ is calculated using (28).
- **Step 3: Robust beamforming optimization:** first, the phase-shift matrix, total iteration times, iteration index, terminating condition and objective value are initialized. Then, (37) and problem (41) are iteratively solved by bisection method and SDR/BnB to optimize μ and Θ , until the optimization procedure converges.
- **Step 4: Output solutions:** the optimal Lagrange dual variable, worst-case CSI error, optimal transmit and passive beamforming are obtained and output.

C. Computational Complexity Analysis

Here we analyse the approximate computational complexity of **Algorithm 1** through the comparisons with the following benchmarks:

- 1) **Benchmark 1 (B1):** the non-robust approach in [26], which directly uses the estimated CSI depending on angle-of-departure/arrival to design the beams, without considering the CSI errors.
- 2) **Benchmark 2 (B2):** the worst-case robust beamforming optimization algorithms in [27] or [28] based on S-procedure and penalty CCP.

Table I lists the approximate computational complexities of our algorithm and **B1**, **B2**, where

- 1) $o_\mu \approx \mathcal{O}(\log_2 W_\mu)$ is the complexity of the bisection method, which is used to find the optimal μ from (37), where W_μ denotes the length of the search interval.
- 2) $o_{(SDR)} \approx \mathcal{O}((N+1)^4 N^{\frac{1}{2}} \log_2 \frac{1}{\epsilon_{(SDR)}})$ is the complexity of SDR [39], which is used to solve problem (41), where $\epsilon_{(SDR)} > 0$ represents the solution accuracy.

Algorithm 1: Proposed Overall Optimization Algorithm.

Input: $q_1, v_1, \hat{p}, d_{BS}, d_{RIS}, \lambda, M, L, N, \epsilon_{\Delta p}$;
 Compute \mathbf{H}_{B-R} and $\hat{\mathbf{h}}_{R-M}$ according to (5) and (6);
 % Begin computation for the CSI error bound;
 Compute CSI error bound $\epsilon_{\Delta h_{R-M}}$ using (28);
 % Begin optimization;
 Initialize: $\theta_1 = \theta_2 = \dots = \theta_N = 0$, total iteration times T , iteration index $t = 1$, terminating condition ϵ_R , initial objective value $R_{Record}^{obj} = 0$;
while $t \leq T$ **do**
 Record the t -th Θ : $\Theta_{Record} \leftarrow \Theta$;
 Solve (37) by using bisection method with given Θ , and then obtain $\bar{\mu}$;
 Compute \mathbf{Y} and \mathbf{X} ;
 Solve problem (41) using BnB/SDR method, obtain Θ and the value of objective function R^{obj} ;
if $|R^{obj} - R_{Record}^{obj}| \leq \epsilon_R$, **then**
break;
 $t \leftarrow t + 1$;
 Record the t -th R^{obj} : $R_{Record}^{obj} \leftarrow R^{obj}$;
 Obtain $\bar{\mu}$;
 Obtain the optimal Θ : $\bar{\Theta} \leftarrow \Theta$;
 Compute $\bar{\Delta h}_{R-M}(\bar{\mu}, \bar{\Theta})$ using (36);
 Compute $\bar{\mathbf{w}}$ using (29);
Output: $\bar{\Theta}, \bar{\mathbf{w}}$;

- 3) $o_{(BnB)} \approx \left(\prod_{i=1}^N \lceil \frac{2(\ell_u - \ell_l)}{\delta} \rceil \right) o_{(SDR)}$ is the complexity of BnB, which is used to solve problem (41), where δ is specified in [Lemma 4, 40].
- 4) $o_{\mathbf{w}} \approx \mathcal{O}((NM + M + 2)^{\frac{1}{2}} M[M^2 + M((NM + 1)^2 + (1 + M)^2) + ((NM + 1)^3 + (1 + M)^3)])$ and $o_{\Theta} \approx \mathcal{O}((NM + 2 + 2N)^{\frac{1}{2}} N[N^2 + N((NM + 1)^2 + 1) + ((NM + 1)^3 + 1) + N^2])$ are the complexities of the transmit beamforming optimization and passive beamforming optimization of **B2**.
- 5) T_P^{Con} and T_R^{Con} stand for the total iteration times required for the convergence of **Algorithm 1** and **B2**.

Table I indicates that: 1) **B1** requires only one time of SDR optimization. It is the simplest approach but may suffer from serious performance degradation in the presence of CSI errors. 2) In each iteration, **B2** is more computationally complex than the proposed algorithm with SDR, whereas their overall complexities depend on the total iteration times for convergence. However, since the solutions of both the two subproblems in our proposed approach are theoretically optimal, our algorithm may converge faster and require less iterations than **B2**. This will be validated from the perspective of convergence rate in Section V-C. 3) Although the proposed algorithm with BnB is also computationally complicated in one iteration, it has the advantages of providing near-optimal solutions and dealing with arbitrary phase shift argument sets. These advantages will be numerically justified in Section V-C as well.

V. SIMULATION RESULTS

In this section, the system parameters are configured and the performance metric is defined. Then, the CSI error bound, derived in Section III, is numerically investigated. Finally, the performance of **Algorithm 1** is evaluated and compared with those of **B1** and **B2**, in terms of the worst-case SNR at the MU and the algorithm efficiency.

TABLE I: Approximate computational complexities.

Algorithms	Approximate complexities per iteration	Overall complexities
Proposed algorithm with SDR	$o_\mu + o_{(SDR)}$	$(o_\mu + o_{(SDR)}) \times T_P^{Con}$
Proposed algorithm with BnB	$o_\mu + o_{(BnB)}$	$(o_\mu + o_{(BnB)}) \times T_P^{Con}$
Robust beamforming in [27] or [28] (B2)	$o_w + o_\Theta$	$(o_w + o_\Theta) \times T_R^{Con}$
Non-robust beamforming in [26] (B1)	$o_{(SDR)}$	$o_{(SDR)}$

A. System Parameters and Performance Metric

1) *System Parameters*: In the simulations, the system parameters are set as follows. \mathbf{q}_1 , \mathbf{v}_1 and $\hat{\mathbf{p}}$ are set as $\mathbf{q}_1 = (0, 0, 25)^T$, $\mathbf{v}_1 = (2, -2, 26)^T$ and $\hat{\mathbf{p}} = (10, 5, 18)^T$ in meters. The antenna/element spacing is $d_{BS} = d_{RIS} = 0.5$ cm. The number of transmit antennas is $M = 32$. The total transmit power is $P_T = 27$ dBm. The noise power at the receiver side is $\sigma_n^2 = -80$ dBm. The carrier frequency is $f_c = 60$ GHz. The speed of light is $c \approx 2.99792458 \times 10^8$ m/s. The signal wavelength is calculated by $\lambda = \frac{c}{f_c}$. For the large-scale path loss, we set $\zeta_0 = -30$ dB, $d_0 = 1$ m, and $\alpha = 2.2$ [31], [33]. The Rician factor is $\kappa_R = 20$. The ℓ_2 -norm of \mathbf{h}_{R-M}^{NLoS} is $\delta_{R-M}^{NLoS} = 10^{-4}$. When performing **Algorithm 1**, we set $T = 4$, $\epsilon_R = 0.0001$, and set the maximum of total iteration times of BnB as 1000, the error tolerance of BnB as $\epsilon_{BnB} = 0.0002$. In addition, the user location error bound $\epsilon_{\Delta p}$ and the number of reflecting elements N (or L) will vary for diverse observations.

2) *Performance Metric*: For evaluating the performance of the proposed algorithm, the worst-case SNR at the MU with respect to the optimized transmit and passive beamforming is considered as a performance metric:

$$S_w(\bar{\Theta}, \bar{\mathbf{w}}) = \frac{P_T |(\mathbf{h}_{R-M}^{worst})^H \bar{\Theta} \mathbf{H}_{B-R} \bar{\mathbf{w}}|^2}{\sigma_n^2}, \quad (45)$$

which is a function of $\bar{\Theta}$ and $\bar{\mathbf{w}}$, where $\mathbf{h}_{R-M}^{worst} = \hat{\mathbf{h}}_{R-M} + \Delta \mathbf{h}_{R-M}(\bar{\mu}, \bar{\Theta})$ is the worst-case channel from RIS to MU. In the simulation results, $S_w(\bar{\Theta}, \bar{\mathbf{w}})$ is presented as original ratio value instead of decibel (dB).

B. CSI Error Bound

Based on the system setup, we first numerically verify the theoretical derivation of the CSI error bound in Section III. Specifically, we compare the following two results to examine the tightness of the CSI error bound:

- 1) $\epsilon_{\Delta h_{R-M}}$, which is theoretically derived from (28).
- 2) The actual CSI error bound, which is obtained by finding the maximum of $\|\Delta \mathbf{h}_{R-M}\|_2$ from 50000 computations of $\|\Delta \mathbf{h}_{R-M}\|_2 = \|\mathbf{h}_{R-M} - \hat{\mathbf{h}}_{R-M}\|_2$, where each computation corresponds to one channel realization of \mathbf{h}_{R-M} with a random \mathbf{p} in the spherical uncertainty region of $\|\Delta \mathbf{p}\|_2 \leq \epsilon_{\Delta p}$.

Fig. 3 depicts the CSI error bounds with respect to N and $\epsilon_{\Delta p}$. It indicates that first, the overall theoretical results fit well with the actual ones, implying that the derivation of the CSI error bound is correct. Second, the CSI error bounds increase as N or $\epsilon_{\Delta p}$ grows, illustrating that more reflecting elements or higher level of user location uncertainty will lead to graver CSI error. Third, the red dashed curves are always below the blue solid curves, manifesting that the theoretical results are upper bounds of the corresponding actual results, which become tight when the level of the user location uncertainty is not significantly high.

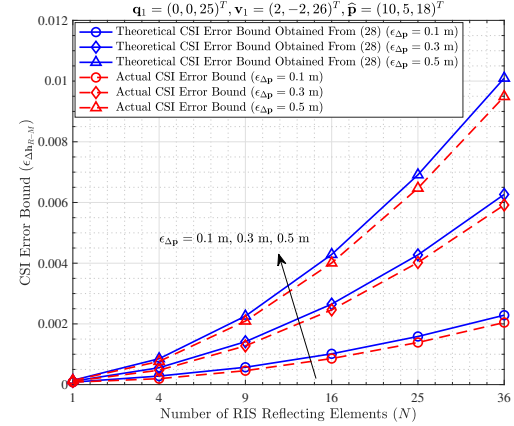
Fig. 3: The CSI error bounds as functions of N with different $\epsilon_{\Delta p}$.

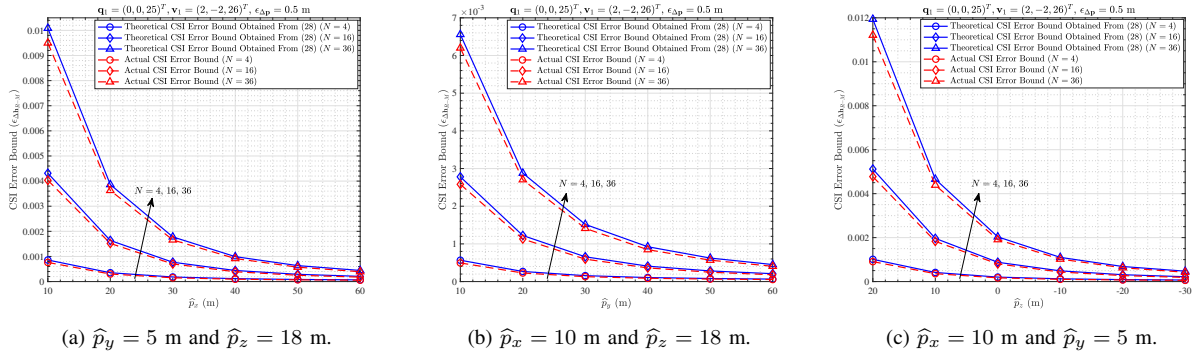
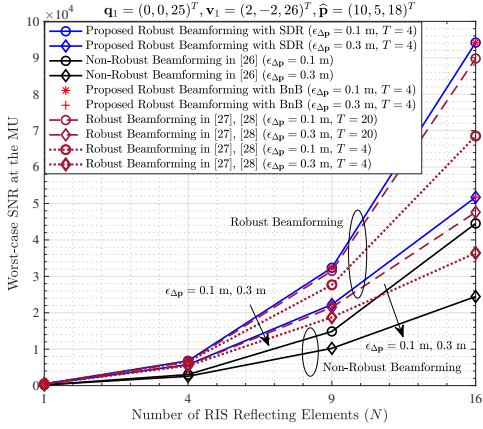
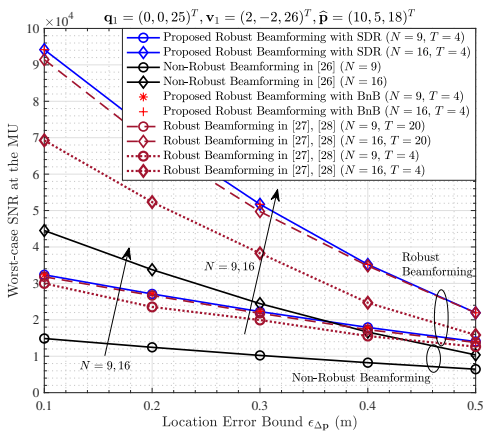
Fig. 4 displays the CSI error bounds with respect to user coordinates, with $\epsilon_{\Delta p} = 0.5$ m and different N . It demonstrates that when the distance between RIS and MU increases while the user location error bound is fixed, the theoretical CSI error bounds descend and become tighter.

C. Algorithm Performance Evaluation

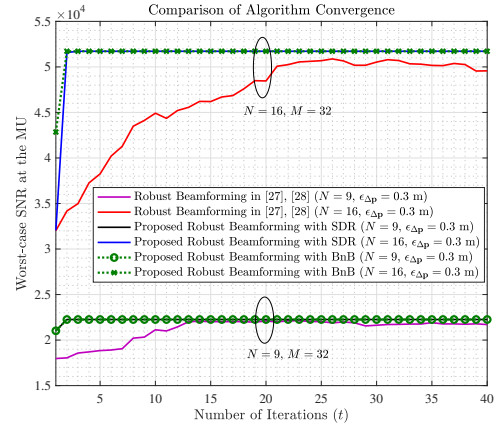
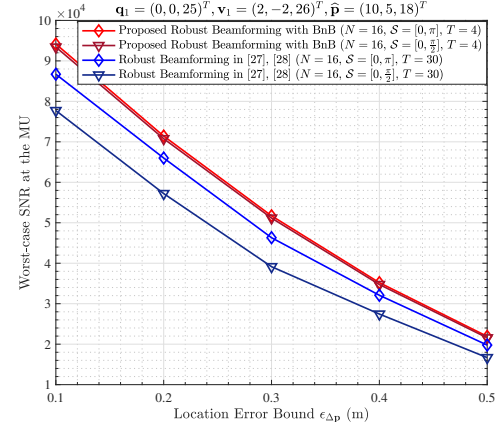
Subsequently, we investigate the performance of the proposed algorithm through the comparisons with **B1** and **B2**, in terms of both the worst-case SNR and the algorithm efficiency. As **B1** and **B2** can only apply to the phase shift argument set of $[0, 2\pi]$, here we first compare the performances under the condition of $\mathcal{S} = [0, 2\pi]$, and then justify the advantages of our algorithm with BnB in the cases of other $\mathcal{S} = [\ell_l, \ell_u]$.

Fig. 5 and Fig. 6 show the worst-case SNRs at the MU with respect to N and $\epsilon_{\Delta p}$ when $\mathcal{S} = [0, 2\pi]$. Results reveal that: 1) the worst-case SNRs at the MU are strongly influenced by the number of the RIS reflecting elements and the level of the CSI uncertainty. 2) The proposed approach significantly outperforms the non-robust approach, i.e. **B1**, thus validating the robustness of our algorithm. 3) The proposed approach performs better than **B2**. This is because the solutions of two subproblems in our algorithm are both theoretically optimal, so that after sufficient times of iterations, the eventual outcomes of our algorithm converge on the global optima. However, it can also be seen that if T is large enough, the worst-case SNRs of **B2** are close to those of the proposed algorithm. Thereupon, we will evaluate the performance from the perspective of the convergence rate as well, in order to show a more comprehensive comparison.

Fig. 7 plots the convergence rates of the proposed algorithm and **B2** when $\mathcal{S} = [0, 2\pi]$, showing that the proposed algorithm converges after around $T_P^{Con} = 3$ iterations, while **B2** converges after around $T_R^{Con} = 20$ iterations. This demonstrates that our algorithm outperforms **B2** in terms of the convergence rate, illustrating meanwhile that our proposed design would be more advantageous in practical applications.

Fig. 4: The CSI error bounds as functions of user coordinates with $\epsilon_{\Delta p} = 0.5$ m and different N .Fig. 5: Worst-case SNRs at the MU with respect to N when $\mathcal{S} = [0, 2\pi]$.Fig. 6: Worst-case SNRs at the MU with respect to $\epsilon_{\Delta p}$ when $\mathcal{S} = [0, 2\pi]$.

Finally, in order to justify that the proposed algorithm with BnB possesses the advantage of handling arbitrary phase shift argument sets, we take $\mathcal{S} = [\ell_l, \ell_u]$ as an example, and investigate the performances of **B2** and the proposed algorithm with BnB in the cases of $\mathcal{S} = [0, \pi]$ and $\mathcal{S} = [0, \frac{\pi}{2}]$. Since the solutions of **B2** intrinsically belong to $[0, 2\pi]$, we perform the rounding operations for $\theta_{\ell+(k-1)L}$ to map the arguments into $\theta_{\ell+(k-1)L} \in [0, \pi]$ and $\theta_{\ell+(k-1)L} \in [0, \frac{\pi}{2}]$ after running **B2**. Specifically, under the argument constraint of $\mathcal{S} = [0, \pi]$, we

Fig. 7: Comparisons of the convergence rates of the proposed algorithm and **B2**, when $\mathcal{S} = [0, 2\pi]$, $N = 9, 16$ and $\epsilon_{\Delta p} = 0.3$ m.Fig. 8: Worst-case SNRs at the MU when the phase shift argument sets are $\mathcal{S} = [0, \pi]$ and $\mathcal{S} = [0, \frac{\pi}{2}]$.

perform

$$\begin{cases} \theta_{\ell+(k-1)L} = \pi, & \text{if } \theta_{\ell+(k-1)L} \in (\pi, \frac{3\pi}{2}); \\ \theta_{\ell+(k-1)L} = 0, & \text{if } \theta_{\ell+(k-1)L} \in [\frac{3\pi}{2}, 2\pi], \end{cases} \quad (46)$$

and under the argument constraint of $\mathcal{S} = [0, \frac{\pi}{2}]$, we perform

$$\begin{cases} \theta_{\ell+(k-1)L} = \frac{\pi}{2}, & \text{if } \theta_{\ell+(k-1)L} \in (\frac{\pi}{2}, \frac{5\pi}{4}); \\ \theta_{\ell+(k-1)L} = 0, & \text{if } \theta_{\ell+(k-1)L} \in [\frac{5\pi}{4}, 2\pi]. \end{cases} \quad (47)$$

Fig. 8 depicts the worst-case SNRs at the MU with the two phase shift argument sets, demonstrating that when $\mathcal{S} \neq [0, 2\pi]$, the BnB can still maintain good SNR performance, whereas **B2** performs worse as **B2** only applies to the phase shift argument

constraint of $\mathcal{S} = [0, 2\pi]$.

VI. CONCLUSIONS AND PROSPECTS

In this paper, when adopting the user location to acquire the CSI in the RIS-aided wireless communication system, we theoretically derived an approximate CSI error bound in the presence of user location uncertainty, with the aid of Taylor approximation, triangle and power mean inequalities, and SDR method. Then, in order to resist the impact of location error on the beamforming design, we formulated a worst-case robust beamforming optimization problem to jointly optimize the transmit and passive beamforming. To solve this non-convex problem efficiently, we proposed an iterative optimization approach based on Lagrange multiplier and matrix inverse lemma, and evaluated its performance in terms of the worst-case SNR at the MU and the algorithm efficiency. Results verified the theoretical derivation of the CSI error bound, and validated the robustness of the proposed approach. Compared with the existing S-procedure and penalty CCP based robust beamforming techniques, our algorithm performed better and converged faster. Consequently, the proposed design in this work is promising in contributing to the development of location information assisted RIS-aided communications.

APPENDIX A PROOF OF LEMMA 1

In Appendix A, we prove the results in Lemma 1. Since the cosine term in (19) is the dominant factor that makes the derivation for the maximum of $\Omega(\Delta\mathbf{p})$ become challenging, we first apply the fourth-order Taylor expansion of $\cos x \approx 1 - \frac{1}{2!}x^2 + \frac{1}{4!}x^4$ at $x = 0$ to approximate $\cos(\frac{2\pi}{\lambda}\mathfrak{U}_{\ell+(k-1)L})$, and obtain

$$\cos\left(\frac{2\pi}{\lambda}\mathfrak{U}_{\ell+(k-1)L}\right) \approx 1 - \frac{2\pi^2}{\lambda^2}\mathfrak{U}_{\ell+(k-1)L}^2 + \frac{2\pi^4}{3\lambda^4}\mathfrak{U}_{\ell+(k-1)L}^4. \quad (48)$$

Substituting (48) into (19), after some manipulations, we have

$$\Omega(\Delta\mathbf{p}) \approx T_1(\Delta\mathbf{p}) + T_2(\Delta\mathbf{p}), \quad (49)$$

where $T_1(\Delta\mathbf{p})$ and $T_2(\Delta\mathbf{p})$ are expressed as (50) and (51) on the top of the next page.

Note that because $\cos(\frac{2\pi}{\lambda}\mathfrak{U}_{\ell+(k-1)L}) \leq 1$, we have $1 - \frac{2\pi^2}{\lambda^2}\mathfrak{U}_{\ell+(k-1)L}^2 + \frac{2\pi^4}{3\lambda^4}\mathfrak{U}_{\ell+(k-1)L}^4 \leq 1$, yielding $\frac{4\pi^2}{\lambda^2}\mathfrak{U}_{\ell+(k-1)L}^2 - \frac{4\pi^4}{3\lambda^4}\mathfrak{U}_{\ell+(k-1)L}^4 \geq 0$. Therefore, by utilizing the triangle inequality of $\|\mathbf{v}_{\ell+(k-1)L} - \hat{\mathbf{p}} - \Delta\mathbf{p}\|_2 \geq \|\mathbf{v}_{\ell+(k-1)L} - \hat{\mathbf{p}}\|_2 - \|\Delta\mathbf{p}\|_2 \geq \|\mathbf{v}_{\ell+(k-1)L} - \hat{\mathbf{p}}\|_2 - \epsilon_{\Delta\mathbf{p}}$, we have $\|\mathbf{v}_{\ell+(k-1)L} - \hat{\mathbf{p}} - \Delta\mathbf{p}\|_2^{-\frac{\alpha}{2}} \leq (\|\mathbf{v}_{\ell+(k-1)L} - \hat{\mathbf{p}}\|_2 - \epsilon_{\Delta\mathbf{p}})^{-\frac{\alpha}{2}}$ because α is positive, and obtain an upper bound of $\Omega(\Delta\mathbf{p})$, denoted by $\Omega_1(\Delta\mathbf{p})$, as

$$\Omega(\Delta\mathbf{p}) \leq \Omega_1(\Delta\mathbf{p}) = T_1(\Delta\mathbf{p}) + T_2^{\text{UPP}}(\Delta\mathbf{p}), \quad (52)$$

where $T_2^{\text{UPP}}(\Delta\mathbf{p})$ is specified in (53) on the top of the next page, which is an upper bound of $T_2(\Delta\mathbf{p})$.

Subsequently, as it is still difficult to derive the maximum of $\Omega_1(\Delta\mathbf{p})$ under the constraint of $\|\Delta\mathbf{p}\|_2 \leq \epsilon_{\Delta\mathbf{p}}$, we focus on finding an approximation of $T_1(\Delta\mathbf{p})$. As the value of α is generally around 2 in the sparse geometry channel model [33], the second-order Taylor approximation for $T_1(\Delta\mathbf{p})$ can

be sufficiently accurate. Therefore, by using the second-order Taylor expansion:

$$T_1(\Delta\mathbf{p}) \approx T_1(\mathbf{0}) + (\nabla T_1(\mathbf{0}))^T \Delta\mathbf{p} + \frac{1}{2}\Delta\mathbf{p}^T \nabla^2 T_1(\mathbf{0}) \Delta\mathbf{p}$$

at $\Delta\mathbf{p} = \mathbf{0}$ to approximate $T_1(\Delta\mathbf{p})$, and after a few manipulations, we have

$$\Omega_1(\Delta\mathbf{p}) \approx \Delta\mathbf{p}^T \mathbf{R} \Delta\mathbf{p} + T_3(\Delta\mathbf{p}), \quad (54)$$

where \mathbf{R} is given by (23) in Lemma 1, while $T_3(\Delta\mathbf{p})$ is expressed as (55) on the top of the next page.

In (55), because a quadratic function with respect to $\Delta\mathbf{p}$ appears as its square form inside the summation operator in $T_3(\Delta\mathbf{p})$, we use the power mean inequality, i.e. $\frac{1}{N} \sum_{i=1}^N x_i \leq \sqrt{\frac{1}{N} \sum_{i=1}^N x_i^2}$ for $x_i \geq 0$ to derive an upper bound of $T_3(\Delta\mathbf{p})$, denoted by $T_3^{\text{UPP}}(\Delta\mathbf{p})$, and obtain (56) on the top of the next page, where \mathbf{S} is detailed in (22) in Lemma 1. Thus, $\Omega_1(\Delta\mathbf{p})$ is upper bounded by

$$\Omega_1(\Delta\mathbf{p}) \leq \Omega_2(\Delta\mathbf{p}) = \Delta\mathbf{p}^T \mathbf{R} \Delta\mathbf{p} - \frac{4\pi^4}{3\lambda^4 N} (\Delta\mathbf{p}^T \mathbf{S} \Delta\mathbf{p})^2. \quad (55)$$

Consequently, we have $\Omega(\Delta\mathbf{p}) \leq \Omega_1(\Delta\mathbf{p}) \leq \Omega_2(\Delta\mathbf{p})$, indicating that $\Omega_2(\Delta\mathbf{p})$ is an approximate upper bound of $\Omega(\Delta\mathbf{p})$. In order to acquire the maximum of $\Omega_2(\Delta\mathbf{p})$ under the constraint of $\|\Delta\mathbf{p}\|_2 \leq \epsilon_{\Delta\mathbf{p}}$, we can formulate the following maximization problem:

$$\max_{\Delta\mathbf{p}} \Omega_2(\Delta\mathbf{p}) = \Delta\mathbf{p}^T \mathbf{R} \Delta\mathbf{p} - \frac{4\pi^4}{3\lambda^4 N} (\Delta\mathbf{p}^T \mathbf{S} \Delta\mathbf{p})^2, \quad (58a)$$

$$\text{s.t. } \|\Delta\mathbf{p}\|_2 \leq \epsilon_{\Delta\mathbf{p}}. \quad (58b)$$

By defining $\mathbf{P} = \Delta\mathbf{p}\Delta\mathbf{p}^T$ and using SDR, problem (58) can be further transformed by dropping the rank-one constraint into problem (21) in Lemma 1. Problem (21) is convex, because: 1) the $\text{tr}(\cdot)$ is linear, while the $-(\cdot)^2 + (\cdot)$ is concave, making the objective function in (21a) concave with respect to $\Delta\mathbf{p}$; 2) the constraint (21b) is convex. Hence, it can be solved by CVX, after which the maximum of $\Omega_2(\Delta\mathbf{p})$ under $\|\Delta\mathbf{p}\|_2 \leq \epsilon_{\Delta\mathbf{p}}$ can be derived. Because $\Omega_2(\Delta\mathbf{p})$ is an approximate upper bound of $\Omega(\Delta\mathbf{p})$, the maximum of $\Omega_2(\Delta\mathbf{p})$ is also an approximate upper bound of the maximum of $\Omega(\Delta\mathbf{p})$, which completes the proof of Lemma 1.

APPENDIX B PROOF OF PROPOSITION 1

In Appendix B, we prove that problem (38) can be transformed into an argument and unit-modulus constrained QCQP problem. Here, the existence of $(\Theta \mathbf{H}_{B-R} \mathbf{H}_{B-R}^H \Theta^H + \bar{\mu} \mathbf{I})^{-1}$ is the primary factor that makes problem (38) tough to compute. Fortunately, as $\bar{\mu} \mathbf{I}$ is invertible, $(\Theta \mathbf{H}_{B-R} \mathbf{H}_{B-R}^H \Theta^H + \bar{\mu} \mathbf{I})^{-1}$ can be further expanded with the aid of the matrix inverse lemma. Although the matrix inverse lemma generally leads to an expansion in a more complicated form, it is remarkable that in problem (38), we have $\Theta^H \Theta = \mathbf{I}$, which can potentially make the expansion become rather simple.

According to the matrix inverse lemma, we have

$(\mathbf{A} + \mathbf{U}\mathbf{B}\mathbf{V})^{-1} = \mathbf{A}^{-1} - \mathbf{A}^{-1}\mathbf{U}\mathbf{B}(\mathbf{I} + \mathbf{V}\mathbf{A}^{-1}\mathbf{U}\mathbf{B})^{-1}\mathbf{V}\mathbf{A}^{-1}$, if \mathbf{A} is invertible. Hence, let $\mathbf{A} = \bar{\mu} \mathbf{I}$, $\mathbf{U}\mathbf{B} = \Theta \mathbf{H}_{B-R}$ and $\mathbf{V} = \mathbf{H}_{B-R}^H \Theta^H$. Then, we obtain (59) on the top of the next page. Eq. (59) indicates that $(\Theta \mathbf{H}_{B-R} \mathbf{H}_{B-R}^H \Theta^H + \bar{\mu} \mathbf{I})^{-1}$ can

$$T_1(\Delta \mathbf{p}) = \sum_{k=1}^L \sum_{\ell=1}^L \left\{ \|\mathbf{v}_{\ell+(k-1)L} - \hat{\mathbf{p}} - \Delta \mathbf{p}\|_2^{-\alpha} + \|\mathbf{v}_{\ell+(k-1)L} - \hat{\mathbf{p}}\|_2^{-\alpha} - 2 \|\mathbf{v}_{\ell+(k-1)L} - \hat{\mathbf{p}} - \Delta \mathbf{p}\|_2^{-\frac{\alpha}{2}} \|\mathbf{v}_{\ell+(k-1)L} - \hat{\mathbf{p}}\|_2^{-\frac{\alpha}{2}} \right\}, \quad (50)$$

$$T_2(\Delta \mathbf{p}) = \sum_{k=1}^L \sum_{\ell=1}^L \left\{ \|\mathbf{v}_{\ell+(k-1)L} - \hat{\mathbf{p}} - \Delta \mathbf{p}\|_2^{-\frac{\alpha}{2}} \|\mathbf{v}_{\ell+(k-1)L} - \hat{\mathbf{p}}\|_2^{-\frac{\alpha}{2}} \left(\frac{4\pi^2}{\lambda^2} \mathfrak{U}_{\ell+(k-1)L}^2 - \frac{4\pi^4}{3\lambda^4} \mathfrak{U}_{\ell+(k-1)L}^4 \right) \right\}. \quad (51)$$

$$T_2^{\text{UPP}}(\Delta \mathbf{p}) = \sum_{k=1}^L \sum_{\ell=1}^L \left\{ \left(\|\mathbf{v}_{\ell+(k-1)L} - \hat{\mathbf{p}}\|_2 - \epsilon_{\Delta \mathbf{p}} \right)^{-\frac{\alpha}{2}} \|\mathbf{v}_{\ell+(k-1)L} - \hat{\mathbf{p}}\|_2^{-\frac{\alpha}{2}} \left(\frac{4\pi^2}{\lambda^2} \mathfrak{U}_{\ell+(k-1)L}^2 - \frac{4\pi^4}{3\lambda^4} \mathfrak{U}_{\ell+(k-1)L}^4 \right) \right\}. \quad (53)$$

$$T_3(\Delta \mathbf{p}) = -\frac{4\pi^4}{3\lambda^4} \sum_{k=1}^L \sum_{\ell=1}^L \left\{ \left[\Delta \mathbf{p}^T \left(\|\mathbf{v}_{\ell+(k-1)L} - \hat{\mathbf{p}}\|_2 - \epsilon_{\Delta \mathbf{p}} \right)^{-\frac{\alpha}{4}} \|\mathbf{v}_{\ell+(k-1)L} - \hat{\mathbf{p}}\|_2^{-\frac{\alpha}{4}} \mathbf{\Xi}_{\ell+(k-1)L} \Delta \mathbf{p} \right]^2 \right\}. \quad (55)$$

$$T_3(\Delta \mathbf{p}) \leq T_3^{\text{UPP}}(\Delta \mathbf{p}) = -\frac{4\pi^4}{3\lambda^4 N} \left(\sum_{k=1}^L \sum_{\ell=1}^L \left\{ \Delta \mathbf{p}^T \left(\|\mathbf{v}_{\ell+(k-1)L} - \hat{\mathbf{p}}\|_2 - \epsilon_{\Delta \mathbf{p}} \right)^{-\frac{\alpha}{4}} \|\mathbf{v}_{\ell+(k-1)L} - \hat{\mathbf{p}}\|_2^{-\frac{\alpha}{4}} \mathbf{\Xi}_{\ell+(k-1)L} \Delta \mathbf{p} \right\} \right)^2 = -\frac{4\pi^4}{3\lambda^4 N} (\Delta \mathbf{p}^T \mathbf{S} \Delta \mathbf{p})^2. \quad (56)$$

$$\begin{aligned} (\Theta \mathbf{H}_{B-R} \mathbf{H}_{B-R}^H \Theta^H + \bar{\mu} \mathbf{I})^{-1} &= \bar{\mu}^{-1} \mathbf{I} - \bar{\mu}^{-2} \Theta \mathbf{H}_{B-R} \left(\mathbf{I} + \bar{\mu}^{-1} \mathbf{H}_{B-R}^H \underbrace{\Theta^H \Theta}_{\mathbf{I}} \mathbf{H}_{B-R} \right)^{-1} \mathbf{H}_{B-R}^H \Theta^H \\ &= \bar{\mu}^{-1} \mathbf{I} - \bar{\mu}^{-2} \Theta \mathbf{H}_{B-R} \left(\mathbf{I} + \bar{\mu}^{-1} \mathbf{H}_{B-R}^H \mathbf{H}_{B-R} \right)^{-1} \mathbf{H}_{B-R}^H \Theta^H. \end{aligned} \quad (59)$$

be expanded into an expression, in which Θ is not included in the inverse operator.

Subsequently, using (59), we further simplify $\mathcal{F}(\Theta)$ and $\mathcal{C}(\Theta)$ in problem (38). First, we simplify $\mathcal{F}(\Theta)$. By substituting (59) into (39), we obtain (60) on the top of the next page, where \mathbf{Y} is expressed as

$$\begin{aligned} \mathbf{Y} &= \mathbf{H}_{B-R} - \bar{\mu}^{-1} \mathbf{H}_{B-R} \mathbf{H}_{B-R}^H \mathbf{H}_{B-R} \\ &\quad + \bar{\mu}^{-2} \mathbf{H}_{B-R} \mathbf{H}_{B-R}^H \mathbf{H}_{B-R} \\ &\quad \times (\mathbf{I} + \bar{\mu}^{-1} \mathbf{H}_{B-R}^H \mathbf{H}_{B-R})^{-1} \mathbf{H}_{B-R}^H \mathbf{H}_{B-R}. \end{aligned} \quad (61)$$

Then, we simplify $\mathcal{C}(\Theta)$. By substituting (59) into (40), we obtain (62) on the top of the next page, where \mathbf{X} is given by

$$\begin{aligned} \mathbf{X} &= \bar{\mu}^{-2} \mathbf{H}_{B-R} \mathbf{H}_{B-R}^H \mathbf{H}_{B-R} \mathbf{H}_{B-R}^H - 2\bar{\mu}^{-3} \mathbf{H}_{B-R} \mathbf{H}_{B-R}^H \\ &\quad \times \mathbf{H}_{B-R} (\mathbf{I} + \bar{\mu}^{-1} \mathbf{H}_{B-R}^H \mathbf{H}_{B-R})^{-1} \mathbf{H}_{B-R}^H \mathbf{H}_{B-R} \mathbf{H}_{B-R}^H \\ &\quad + \bar{\mu}^{-4} \mathbf{H}_{B-R} \mathbf{H}_{B-R}^H \mathbf{H}_{B-R} (\mathbf{I} + \bar{\mu}^{-1} \mathbf{H}_{B-R}^H \mathbf{H}_{B-R})^{-1} \\ &\quad \times \mathbf{H}_{B-R}^H \mathbf{H}_{B-R} (\mathbf{I} + \bar{\mu}^{-1} \mathbf{H}_{B-R}^H \mathbf{H}_{B-R})^{-1} \\ &\quad \times \mathbf{H}_{B-R}^H \mathbf{H}_{B-R} \mathbf{H}_{B-R}^H. \end{aligned} \quad (63)$$

Let $\boldsymbol{\theta}$ be defined by $\boldsymbol{\theta} = (e^{j\theta_1}, e^{j\theta_2}, \dots, e^{j\theta_N})^T$. Then, $\mathcal{F}(\Theta)$ and $\mathcal{C}(\Theta)$ can be recast as

$$\begin{aligned} \mathcal{F}(\Theta) &= \hat{\mathbf{h}}_{R-M}^H \Theta \mathbf{Y} \mathbf{Y}^H \Theta^H \hat{\mathbf{h}}_{R-M} \\ &= \boldsymbol{\theta}^T \text{diag}\{\hat{\mathbf{h}}_{R-M}^H\} \mathbf{Y} \mathbf{Y}^H \text{diag}\{\hat{\mathbf{h}}_{R-M}\} \boldsymbol{\theta}^*, \end{aligned} \quad (64)$$

$$\begin{aligned} \mathcal{C}(\Theta) &= \hat{\mathbf{h}}_{R-M}^H \Theta \mathbf{X} \Theta^H \hat{\mathbf{h}}_{R-M} - \epsilon_{\Delta \mathbf{h}_{R-M}}^2 \\ &= \boldsymbol{\theta}^T \text{diag}\{\hat{\mathbf{h}}_{R-M}^H\} \mathbf{X} \text{diag}\{\hat{\mathbf{h}}_{R-M}\} \boldsymbol{\theta}^* - \epsilon_{\Delta \mathbf{h}_{R-M}}^2, \end{aligned} \quad (65)$$

which finally completes the proof of Proposition 1.

REFERENCES

- [1] M. Agiwal, A. Roy and N. Saxena, "Next generation 5G wireless networks: A comprehensive survey," *IEEE Communications Surveys & Tutorials*, vol. 18, no. 3, pp. 1617-1655, Third Quarter 2016.
- [2] C. Liaskos, *et al.*, "A new wireless communication paradigm through software-controlled metasurfaces," *IEEE Communications Magazine*, vol. 56, no. 9, pp. 162-169, Sept. 2018.
- [3] S. Hu, F. Rusek and O. Edfors, "Beyond massive MIMO: The potential of data transmission with large intelligent surfaces," *IEEE Transactions on Signal Processing*, vol. 66, no. 10, pp. 2746-2758, May. 2018.
- [4] M. D. Renzo, *et al.*, "Smart radio environments empowered by reconfigurable intelligent surfaces: How it works, state of research, and the road ahead," *IEEE Journal on Selected Areas in Communications*, vol. 38, no. 11, pp. 2450-2525, Nov. 2020.
- [5] S. Gong, *et al.*, "Toward smart wireless communications via intelligent reflecting surfaces: A contemporary survey," *IEEE Communications Surveys & Tutorials*, vol. 22, no. 4, pp. 2283-2314, Fourth Quarter 2020.
- [6] Q. Wu and R. Zhang, "Towards smart and reconfigurable environment: Intelligent reflecting surface aided wireless network," *IEEE Communications Magazine*, vol. 58, no. 1, pp. 106-112, Jan. 2020.
- [7] C. Huang, *et al.*, "Holographic MIMO surfaces for 6G wireless networks: Opportunities, challenges, and trends," *IEEE Wireless Communications*, vol. 27, no. 5, pp. 118-125, Oct. 2020.
- [8] J. Y. Lau and S. V. Hum, "Reconfigurable transmitarray design approaches for beamforming applications," *IEEE Transactions on Antennas and Propagation*, vol. 60, no. 12, pp. 5679-5689, Dec. 2012.
- [9] L. Dai, *et al.*, "Reconfigurable intelligent surface-based wireless communications: Antenna design, prototyping, and experimental results," *IEEE Access*, vol. 8, pp. 45913-45923, Mar. 2020.
- [10] N. Rajatheva, *et al.*, "White paper on broadband connectivity in 6G," *6G Research Visions*, no. 10, University of Oulu, Jun. 2020.
- [11] E. Björnson, Ö. Özdogan, and E. G. Larsson, "Intelligent reflecting surface versus decode-and-forward: How large surfaces are needed to beat relaying?" *IEEE Wireless Communications Letters*, vol. 9, no. 2, pp. 244-248, Feb. 2020.
- [12] M. Cui, G. Zhang and R. Zhang, "Secure wireless communication via intelligent reflecting surface," *IEEE Wireless Communications Letters*, vol. 8, no. 5, pp. 1410-1414, Oct. 2019.
- [13] C. Guo, Y. Cui, F. Yang and L. Ding, "Outage probability analysis and minimization in intelligent reflecting surface-assisted MISO systems," *IEEE Communications Letters*, vol. 24, no. 7, pp. 1563-1567, Jul. 2020.
- [14] Z. Xing, R. Wang, X. Yuan and J. Wu, "Location-aware beamforming design for reconfigurable intelligent surface aided communication system," in *Proc. IEEE/CIC International Conference on Communications in China*, Xiamen, China, Jul. 2021, pp. 1-6.
- [15] C. Huang, *et al.*, "Reconfigurable intelligent surfaces for energy efficiency in wireless communication," *IEEE Transactions on Wireless Communications*, vol. 18, no. 8, pp. 4157-4170, Aug. 2019.
- [16] Q. Wu and R. Zhang, "Intelligent reflecting surface enhanced wireless network via joint active and passive beamforming," *IEEE Transactions on Wireless Communications*, vol. 18, no. 11, pp. 5394-5409, Nov. 2019.
- [17] Q. Wu and R. Zhang, "Beamforming optimization for wireless network aided by intelligent reflecting surface with discrete phase shifts," *IEEE Transactions on Communications*, vol. 68, no. 3, pp. 1838-1851, Mar. 2020.
- [18] Z. Xing, R. Wang, J. Wu and E. Liu, "Achievable rate analysis and phase shift optimization on intelligent reflecting surface with hardware impairments," *IEEE Transactions on Wireless Communications*, Mar. 2021, DOI: 10.1109/TWC.2021.3068225.
- [19] C. Huang, A. Zappone, M. Debbah and C. Yuen, "Achievable rate maximization by passive intelligent mirrors," in *Proc. IEEE International Conference on Acoustics, Speech and Signal Processing (ICASSP)*, Calgary, AB, Canada, Apr. 2018, pp. 3714-3718.
- [20] X. Hu, *et al.*, "Programmable metasurface-based multicast systems: Design

$$\begin{aligned}
\mathcal{F}(\Theta) &= \left\| \left\{ \hat{\mathbf{h}}_{R-M} - \left[\bar{\mu}^{-1} \mathbf{I} - \bar{\mu}^{-2} \Theta \mathbf{H}_{B-R} \left(\mathbf{I} + \bar{\mu}^{-1} \mathbf{H}_{B-R}^H \mathbf{H}_{B-R} \right)^{-1} \mathbf{H}_{B-R}^H \Theta^H \right] \Theta \mathbf{H}_{B-R} \mathbf{H}_{B-R}^H \Theta^H \hat{\mathbf{h}}_{R-M} \right\}^H \Theta \mathbf{H}_{B-R} \right\|_2^2 \\
&= \left\| \left\{ \hat{\mathbf{h}}_{R-M} - \left[\bar{\mu}^{-1} \Theta \mathbf{H}_{B-R} \mathbf{H}_{B-R}^H \Theta^H \hat{\mathbf{h}}_{R-M} - \bar{\mu}^{-2} \Theta \mathbf{H}_{B-R} \left(\mathbf{I} + \bar{\mu}^{-1} \mathbf{H}_{B-R}^H \mathbf{H}_{B-R} \right)^{-1} \mathbf{H}_{B-R}^H \underbrace{\Theta^H \Theta}_{\mathbf{I}} \mathbf{H}_{B-R} \mathbf{H}_{B-R}^H \Theta^H \hat{\mathbf{h}}_{R-M} \right] \right\}^H \Theta \mathbf{H}_{B-R} \right\|_2^2 \\
&= \left\| \hat{\mathbf{h}}_{R-M}^H \Theta \left[\mathbf{H}_{B-R} - \bar{\mu}^{-1} \mathbf{H}_{B-R} \mathbf{H}_{B-R}^H \mathbf{H}_{B-R} + \bar{\mu}^{-2} \mathbf{H}_{B-R} \mathbf{H}_{B-R}^H \mathbf{H}_{B-R} \left(\mathbf{I} + \bar{\mu}^{-1} \mathbf{H}_{B-R}^H \mathbf{H}_{B-R} \right)^{-1} \mathbf{H}_{B-R}^H \mathbf{H}_{B-R} \right] \right\|_2^2 \\
&= \left\| \hat{\mathbf{h}}_{R-M}^H \Theta \mathbf{Y} \right\|_2^2 = \hat{\mathbf{h}}_{R-M}^H \Theta \underbrace{\mathbf{Y} \mathbf{Y}^H}_{\text{Independent of } \Theta} \Theta^H \hat{\mathbf{h}}_{R-M}.
\end{aligned} \tag{60}$$

$$\begin{aligned}
\mathcal{C}(\Theta) &= \left[\left(\Theta \mathbf{H}_{B-R} \mathbf{H}_{B-R}^H \Theta^H + \bar{\mu} \mathbf{I} \right)^{-1} \Theta \mathbf{H}_{B-R} \mathbf{H}_{B-R}^H \Theta^H \hat{\mathbf{h}}_{R-M} \right]^H \left[\left(\Theta \mathbf{H}_{B-R} \mathbf{H}_{B-R}^H \Theta^H + \bar{\mu} \mathbf{I} \right)^{-1} \Theta \mathbf{H}_{B-R} \mathbf{H}_{B-R}^H \Theta^H \hat{\mathbf{h}}_{R-M} \right] - \epsilon_{\Delta \mathbf{h}_{R-M}}^2 \\
&= \left[\left(\bar{\mu}^{-1} \mathbf{I} - \bar{\mu}^{-2} \Theta \mathbf{H}_{B-R} \left(\mathbf{I} + \bar{\mu}^{-1} \mathbf{H}_{B-R}^H \mathbf{H}_{B-R} \right)^{-1} \mathbf{H}_{B-R}^H \Theta^H \right) \Theta \mathbf{H}_{B-R} \mathbf{H}_{B-R}^H \Theta^H \hat{\mathbf{h}}_{R-M} \right]^H \\
&\quad \times \left[\left(\bar{\mu}^{-1} \mathbf{I} - \bar{\mu}^{-2} \Theta \mathbf{H}_{B-R} \left(\mathbf{I} + \bar{\mu}^{-1} \mathbf{H}_{B-R}^H \mathbf{H}_{B-R} \right)^{-1} \mathbf{H}_{B-R}^H \Theta^H \right) \Theta \mathbf{H}_{B-R} \mathbf{H}_{B-R}^H \Theta^H \hat{\mathbf{h}}_{R-M} \right] - \epsilon_{\Delta \mathbf{h}_{R-M}}^2 \\
&= \left[\bar{\mu}^{-1} \Theta \mathbf{H}_{B-R} \mathbf{H}_{B-R}^H \Theta^H \hat{\mathbf{h}}_{R-M} - \bar{\mu}^{-2} \Theta \mathbf{H}_{B-R} \left(\mathbf{I} + \bar{\mu}^{-1} \mathbf{H}_{B-R}^H \mathbf{H}_{B-R} \right)^{-1} \mathbf{H}_{B-R}^H \underbrace{\Theta^H \Theta}_{\mathbf{I}} \mathbf{H}_{B-R} \mathbf{H}_{B-R}^H \Theta^H \hat{\mathbf{h}}_{R-M} \right]^H \\
&\quad \times \left[\bar{\mu}^{-1} \Theta \mathbf{H}_{B-R} \mathbf{H}_{B-R}^H \Theta^H \hat{\mathbf{h}}_{R-M} - \bar{\mu}^{-2} \Theta \mathbf{H}_{B-R} \left(\mathbf{I} + \bar{\mu}^{-1} \mathbf{H}_{B-R}^H \mathbf{H}_{B-R} \right)^{-1} \mathbf{H}_{B-R}^H \underbrace{\Theta^H \Theta}_{\mathbf{I}} \mathbf{H}_{B-R} \mathbf{H}_{B-R}^H \Theta^H \hat{\mathbf{h}}_{R-M} \right] - \epsilon_{\Delta \mathbf{h}_{R-M}}^2 \\
&= \bar{\mu}^{-2} \hat{\mathbf{h}}_{R-M}^H \Theta \mathbf{H}_{B-R} \mathbf{H}_{B-R}^H \underbrace{\Theta^H \Theta}_{\mathbf{I}} \mathbf{H}_{B-R} \mathbf{H}_{B-R}^H \Theta^H \hat{\mathbf{h}}_{R-M} - \bar{\mu}^{-3} \hat{\mathbf{h}}_{R-M}^H \Theta \mathbf{H}_{B-R} \mathbf{H}_{B-R}^H \underbrace{\Theta^H \Theta}_{\mathbf{I}} \mathbf{H}_{B-R} \left(\mathbf{I} + \bar{\mu}^{-1} \mathbf{H}_{B-R}^H \mathbf{H}_{B-R} \right)^{-1} \\
&\quad \times \mathbf{H}_{B-R}^H \mathbf{H}_{B-R} \mathbf{H}_{B-R}^H \Theta^H \hat{\mathbf{h}}_{R-M} - \bar{\mu}^{-3} \hat{\mathbf{h}}_{R-M}^H \Theta \mathbf{H}_{B-R} \mathbf{H}_{B-R}^H \left(\mathbf{I} + \bar{\mu}^{-1} \mathbf{H}_{B-R}^H \mathbf{H}_{B-R} \right)^{-1} \mathbf{H}_{B-R}^H \underbrace{\Theta^H \Theta}_{\mathbf{I}} \mathbf{H}_{B-R} \mathbf{H}_{B-R}^H \Theta^H \hat{\mathbf{h}}_{R-M} \\
&\quad + \bar{\mu}^{-4} \hat{\mathbf{h}}_{R-M}^H \Theta \mathbf{H}_{B-R} \mathbf{H}_{B-R}^H \mathbf{H}_{B-R} \left(\mathbf{I} + \bar{\mu}^{-1} \mathbf{H}_{B-R}^H \mathbf{H}_{B-R} \right)^{-1} \mathbf{H}_{B-R}^H \underbrace{\Theta^H \Theta}_{\mathbf{I}} \mathbf{H}_{B-R} \left(\mathbf{I} + \bar{\mu}^{-1} \mathbf{H}_{B-R}^H \mathbf{H}_{B-R} \right)^{-1} \mathbf{H}_{B-R}^H \mathbf{H}_{B-R} \mathbf{H}_{B-R}^H \\
&\quad \times \Theta^H \hat{\mathbf{h}}_{R-M} - \epsilon_{\Delta \mathbf{h}_{R-M}}^2 = \hat{\mathbf{h}}_{R-M}^H \Theta \mathbf{X} \Theta^H \hat{\mathbf{h}}_{R-M} - \epsilon_{\Delta \mathbf{h}_{R-M}}^2.
\end{aligned} \tag{62}$$

and analysis," *IEEE Journal on Selected Areas in Communications*, vol. 38, no. 8, pp. 1763-1776, Aug. 2020.

[21] S. Hu, F. Rusek and O. Edfors, "Beyond massive MIMO: The potential of positioning with large intelligent surfaces," *IEEE Transactions on Signal Processing*, vol. 66, no. 7, pp. 1761-1774, Apr. 2018.

[22] J. He, *et al.*, "Large intelligent surface for positioning in millimeter wave MIMO systems," in *Proc. IEEE 91st Vehicular Technology Conference*, Antwerp, Belgium, May 2020, pp. 1-5.

[23] B. Zheng and R. Zhang, "Intelligent reflecting surface-enhanced OFDM: Channel estimation and reflection optimization," *IEEE Wireless Communications Letters*, vol. 9, no. 4, pp. 518-522, Apr. 2020.

[24] L. Wei, *et al.*, "Channel estimation for RIS-empowered multi-user MISO wireless communications," *IEEE Transactions on Communications*, Mar. 2021, DOI: 10.1109/TCOMM.2021.3063236.

[25] Z.-Q. He and X. Yuan, "Cascaded channel estimation for large intelligent metasurface assisted massive MIMO," *IEEE Wireless Communications Letters*, vol. 9, no. 2, pp. 210-214, Feb. 2020.

[26] X. Hu, C. Zhong, Y. Zhang, X. Chen and Z. Zhang, "Location information aided multiple intelligent reflecting surface systems," *IEEE Transactions on Communications*, vol. 68, no. 12, pp. 7948-7962, Dec. 2020.

[27] G. Zhou, C. Pan, H. Ren, K. Wang and A. Nallanathan, "A framework of robust transmission design for IRS-aided MISO communications with imperfect cascaded channels," *IEEE Transactions on Signal Processing*, vol. 68, pp. 5092-5106, Aug. 2020.

[28] G. Zhou, *et al.*, "Robust beamforming design for intelligent reflecting surface aided MISO communication systems," *IEEE Wireless Communications Letters*, vol. 9, no. 10, pp. 1658-1662, Oct. 2020.

[29] J. Zhang, Y. Zhang, C. Zhong and Z. Zhang, "Robust design for intelligent reflecting surfaces assisted MISO systems," *IEEE Communications Letters*, vol. 24, no. 10, pp. 2353-2357, Oct. 2020.

[30] M. Zhao, A. Liu and R. Zhang, "Outage-constrained robust beamforming for intelligent reflecting surface aided wireless communication," *IEEE Transactions on Signal Processing*, vol. 69, pp. 1301-1316, Feb. 2021.

[31] C. Pan, *et al.*, "Intelligent reflecting surface aided MIMO broadcasting for simultaneous wireless information and power transfer," *IEEE Journal on Selected Areas in Communications*, vol. 38, no. 8, pp. 1719-1734, Aug. 2020.

[32] Z. A. Shaban, *et al.*, "Near-field localization with a reconfigurable intelligent surface acting as lens," *arXiv:2010.05617v1*, Oct. 2020.

[33] K. Zhi, C. Pan, H. Ren and K. Wang, "Uplink achievable rate of intelligent reflecting surface-aided millimeter-wave communications with low-resolution ADC and phase noise," *IEEE Wireless Communications Letters*, vol. 10, no. 3, pp. 654-658, Mar. 2021.

[34] D. Hammarwall, M. Bengtsson and B. Ottersten, "Acquiring partial CSI for spatially selective transmission by instantaneous channel norm feedback," *IEEE Transactions on Signal Processing*, vol. 56, no. 3, pp. 1188-1204, Mar. 2008.

[35] E. Björnson and B. Ottersten, "Exploiting long-term statistics in spatially correlated multi-user MIMO systems with quantized channel norm feedback," in *Proc. IEEE International Conference on Acoustics, Speech and Signal Processing*, Las Vegas, NV, USA, Apr. 2008, pp. 3117-3120.

[36] E. Björnson, D. Hammarwall and B. Ottersten, "Exploiting quantized channel norm feedback through conditional statistics in arbitrarily correlated MIMO systems," *IEEE Transactions on Signal Processing*, vol. 57, no. 10, pp. 4027-4041, Oct. 2009.

[37] J. Wang and D. P. Palomar, "Worst-case robust MIMO transmission with imperfect channel knowledge," *IEEE Transactions on Signal Processing*, vol. 57, no. 8, pp. 3086-3100, Aug. 2009.

[38] H. Shen, W. Xu, J. Wang and C. Zhao, "A worst-case robust beamforming design for multi-antenna AF relaying," *IEEE Communications Letters*, vol. 17, no. 4, pp. 713-716, Apr. 2013.

[39] Z.-Q. Luo, *et al.*, "Semidefinite relaxation of quadratic optimization problems," *IEEE Signal Processing Magazine*, vol. 27, no. 3, pp. 20-34, May. 2010.

[40] C. Lu, Z. Deng, W.-Q. Zhang and S.-C. Fang, "Argument division based branch-and-bound algorithm for unit-modulus constrained complex quadratic programming," *Journal of Global Optimization*, vol. 70, pp. 171-187, Aug. 2017.

[41] C. Lu and Y.-F. Liu, "An efficient global algorithm for single-group multicast beamforming," *IEEE Transactions on Signal Processing*, vol. 65, no. 14, pp. 3761-3774, Jul. 2017.

- [42] R. Wang, M. Tao and Y. Huang, "Linear precoding designs for amplify-and-forward multiuser two-way relay systems," *IEEE Transactions on Wireless Communications*, vol. 11, no. 12, pp. 4457-4469, Dec. 2012.
- [43] A. Kaw, J. Paul and M. Keteltas, "Bisection method of solving a nonlinear equation," [Online]. Available: <https://resources.saylor.org/wwwresources/archived/site/wp-content/uploads/2011/11/ME205-3.1-TEXT.pdf>, pp. 1-12, Nov. 2011.